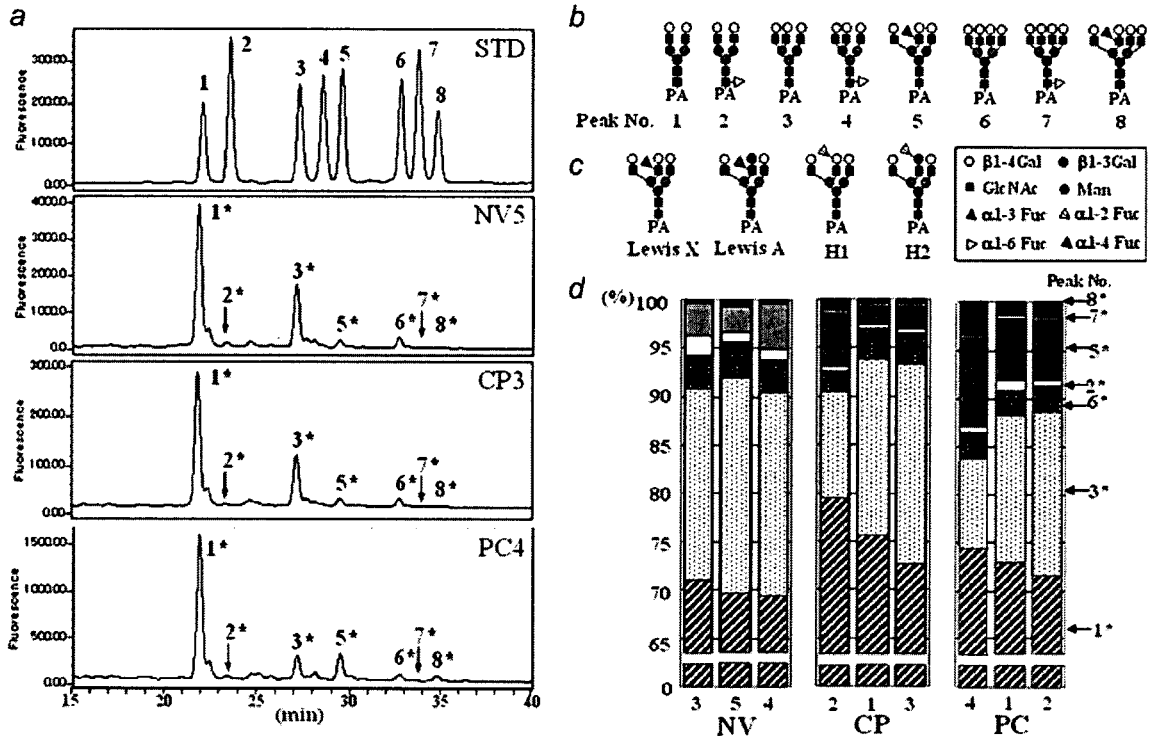

FIGURE 2 – NP-HPLC analysis of PA-labeled *N*-glycans. (*a*) chromatogram of standard PA-labeled *N*-glycans (STD, 10 pmol each) and *N*-glycans released from tryptic peptides of purified haptoglobin (NV5, CP3, and PC4). The peak numbers and the structures of standard PA-labeled *N*-glycans are shown in (*b*). More detailed structures thereof are shown in supplemental Figure 3*a*. (*c*) the candidate structures of *N*-glycan from peak 5*. (*d*) 100% stacked bar graph indicates the percentage of types of detected PA-labeled *N*-glycans derived from purified haptoglobins (NV, CP, and PC; 3 samples each). Fuc, fucose; Gal, galactose; Man, mannose; GlcNAc, *N*-acetylglucosamine; NeuAc, *N*-acetylneuramic acid; PA, 2-aminopyridine.

residues and a Fuc residue are different. To determine the precise structure of the *N*-glycan in peak 5*, sequential exoglycosidase digestion with α1-3/4 fucosidase and β1-4 galactosidase was performed. A Fuc residue and all Gal residues were removed from the *N*-glycan in peak 5*, indicating that the *N*-glycan in peak 5* could be predicted to be a tri-antennary containing a Lewis X type Fuc, which has an α1-3 Fuc and three β1-4 Gals. The detailed procedure and the resultant chromatograms are shown in supplemental Figure 4.

The amount (mol) of *N*-glycans detected in this experiment was calculated based on the peak areas of standard *N*-glycan samples. In each sample, the amount (mol) of each *N*-glycan was summed to 100%, and the results are represented in stacked bar graphs to compare the contribution of each *N*-glycan to the total for each sample (Fig. 2*d*). The average values are shown in supplemental Figure 3*b*. The percentage of each *N*-glycan in the NV samples was similar to previous values reported by Ferens-Sieczkowska and Olczak[7] Although there was not much difference between NV and CP, the composition of *N*-glycans in PC changed markedly. Tri- and tetra-antennary *N*-glycans containing a Lewis X-type Fuc (peaks 5* and 8*) significantly increased in PC.

LC-ESI MS analysis of haptoglobin sialo-glycopeptides at sites 1 and 4

To identify the site responsible for the increase in *N*-glycans containing a Lewis X-type Fuc, site-specific analysis of haptoglobin *N*-glycans was performed in patients with PC, CP and in NV. The tryptic peptide mixture after reduction and alkylation was separated by reverse-phase HPLC followed by ESI MS analysis. Digestion of glycopeptides with a combination of trypsin and lysylendopeptidase should, in theory, yield (Supplemental Fig. 1): Met179-Lsy202, including one *N*-glycan binding site (site 1: Asn184); Asn203-Lsy215, including two *N*-glycan binding sites (site 2 and site 3: Asn207 and Asn211); and, Val236-Lsy251, including one *N*-glycan binding site (site 4: Asn241). The results of these analyses are presented in Figure 3*a*. The representative data shown in Figure 3*a* is the result of the analysis of serum from a normal volunteer (NV 5). Many ions derived from peptides were detected in the base peak chromatogram (BPC, see glossary) shown in Figure 3*a*. The ions detected in the extracted ion chromatogram (EIC, see glossary) of MSMS at *m/z* 657.3, which is the mass number of NeuAc-Gal-GlcNAc, indicated the presence of glycopeptides. Three robust peaks were detected at 40, 61 and 68 min. EIC of the MS scans at the mass number for each site containing a disialo-biantennary *N*-glycan was used to find the elution time for the glycopeptide of each site, because the majority of the *N*-glycans on haptoglobin were disialo-biantennary *N*-glycans. The ion at *m/z* 1221.8–1222.8 represents $[M+4H]^{4+}$ of the glycopeptide containing site 1 with a disialo-biantennary *N*-glycan. The ion at *m/z* 1467.8–1468.8 represents $[M+4H]^{4+}$ of the glycopeptide containing sites 2–3 with two disialo-biantennary *N*-glycans. The ion at *m/z* 1333.9–1334.9 represents $[M+3H]^{3+}$ of the glycopeptide containing site 4 with a disialo-biantennary *N*-glycan. In the three EIC of MS, single peaks were observed at 68 (site 1), 40 (site 2–3) and 61 min (site 4). CP and PC samples were analyzed in the same manner as the NV samples. Averaged MS spectra during 67–72 min of EIC of MS at *m/z* 1221.8–1222.8 (site 1) were performed. The results for NV5, CP4 and PC5 are shown in Figure

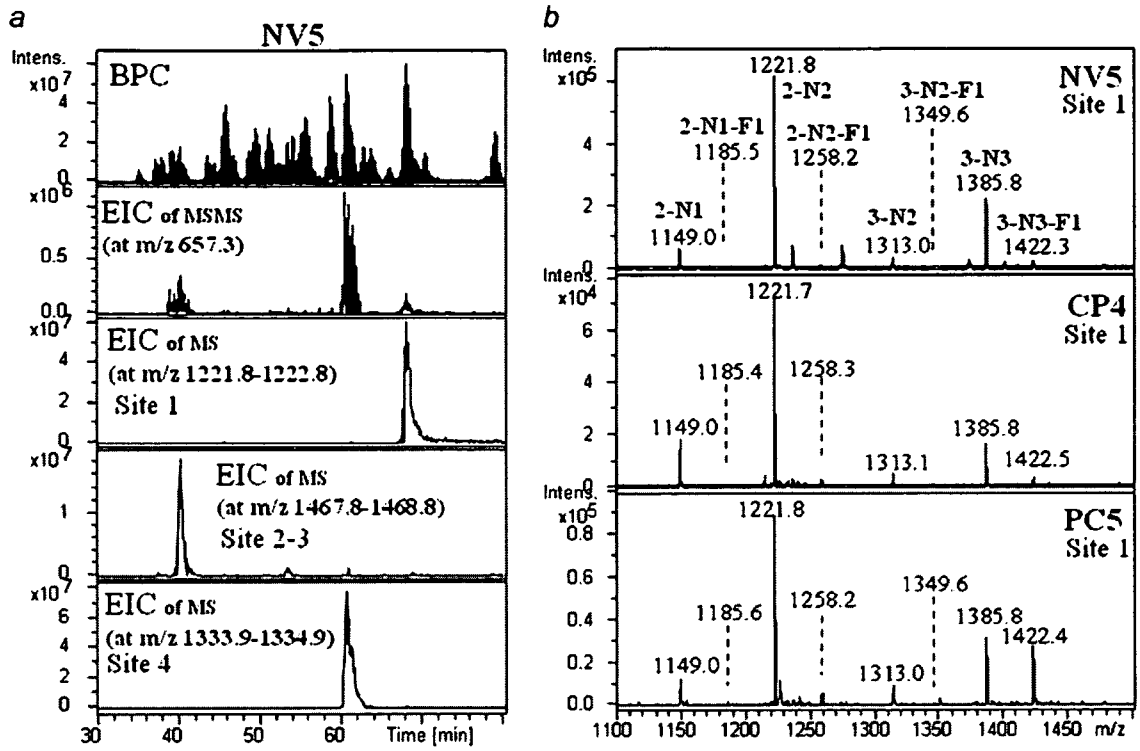

FIGURE 3 – LC-ESI MS analysis of sialo-glycopeptides for sites 1 and 4 on haptoglobin. (*a*) BPC (MS+MSMS), EIC at *m/z* 657.3 (MSMS), EIC at *m/z* 1221.8–1222.8 (MS), EIC at *m/z* 1467.8–1468.8 (MS), and EIC at *m/z* 1333.9–1334.9 (MS) obtained from the analysis of NV5. Scan range for MS: *m/z* 400–3,000, for MSMS: *m/z* 200–3,000. EIC at *m/z* 657.3 suggested the presence of sialo-glycopeptides. EIC at *m/z* 1221.8–1222.8, EIC at *m/z* 1467.8–1468.8 and EIC at *m/z* 1333.9–1334.9 were indicative of: glycopeptides having 2-N2 at site 1; glycopeptide containing both site 2 and 3 with two 2-N2; and glycopeptides having 2-N2 at site 4, respectively. **B**, averaged MS spectra during 67–72 min of EIC at *m/z* 1221.8–1222.8 of MS (site 1) derived from NV5, CP4 and PC 5. Peak abbreviations and structures are summarized in Figure 4.

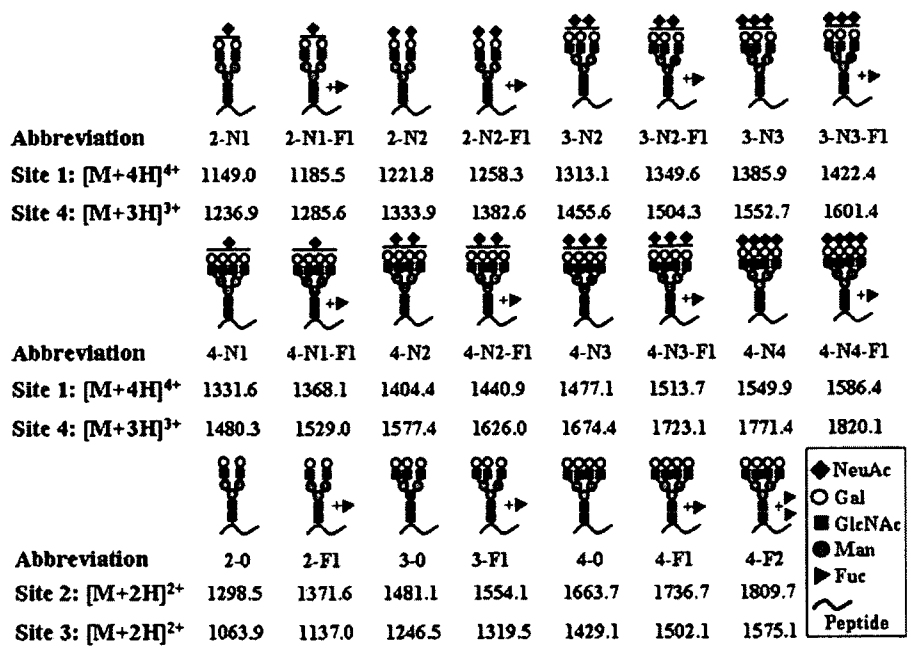

FIGURE 4 – Abbreviations, structures and calculated mass numbers for sialo- or asialo-glycopeptides detected in our study. Sialo-glycopeptides which include site 1 or 4 were calculated as quadruply and triply charged ions, respectively. Asialo-glycopeptides which include site 2 or 3 were calculated as doubly charged ions.

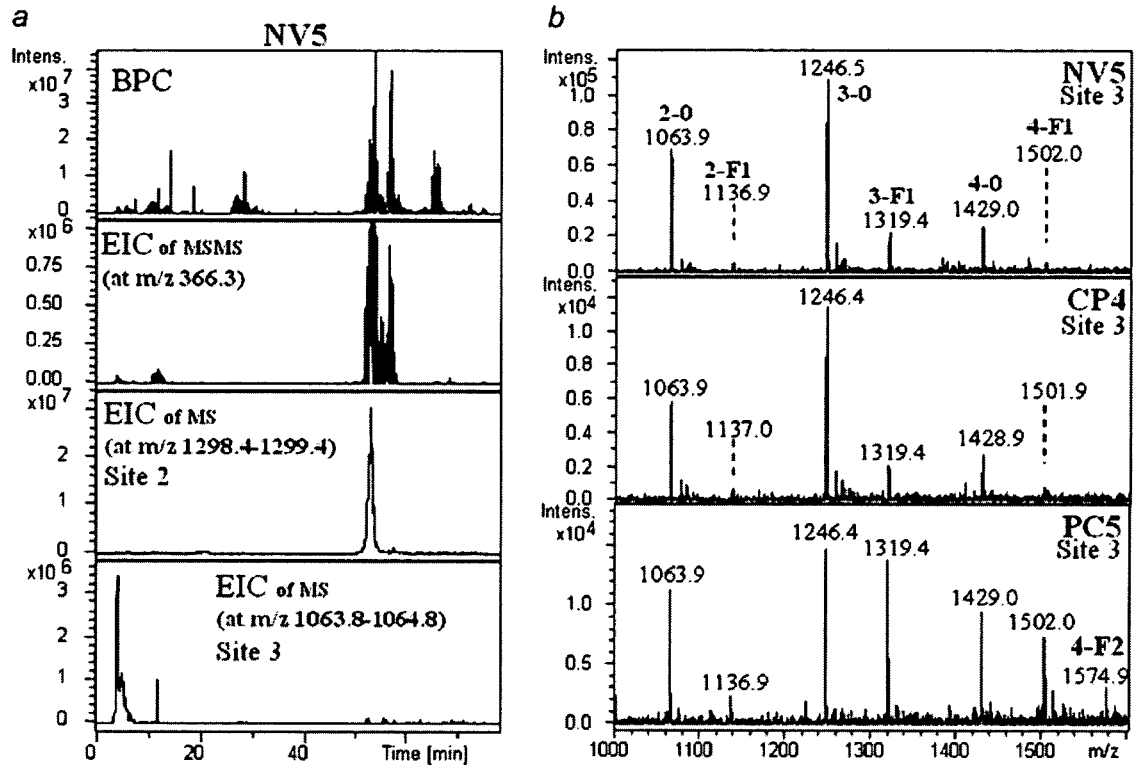

FIGURE 5 – LC-ESI MS analysis of asialo-glycopeptides for sites 2 and 3 on haptoglobin. (*a*) BPC (MS+MSMS), EIC at *m/z* 366.3 (MSMS), EIC at *m/z* 1298.4–1299.4 (MS) and EIC at *m/z* 1063.8–1064.8 (MS), obtained from the analysis of NV5. Scan range for MS: *m/z* 400–3,000, for MSMS: *m/z* 200–3000. EIC at *m/z* 366.3 suggested the presence of asialo-glycopeptides. EIC at *m/z* 1298.4–1299.4 and EIC at *m/z* 1063.8–1064.8 were indicative of glycopeptides having 2-0 at site 2 and site 3, respectively. (*b*) averaged MS spectra during 3–8 min of EIC at *m/z* 1063.8–1064.8 of MS (site 3), derived from NV5, CP4 and PC 5. Peak abbreviations and structures are summarized in Figure 4.

3*b*. The abbreviations for *N*-glycan structures in the glycopeptide are summarized in Figure 4. For example, the peptide containing the tri-antennary *N*-glycan with two NeuAc residues and one Fuc residue is represented as 3-N2-F1. The first numeral indicates the branch number (tri-antennary in this case), N2 indicates the presence of two NeuAc residues, and F1 indicates the presence of one Fuc residue. "0" means the absence of both Fuc and NeuAc. Eight glycopeptides (2-N1, 2-N1-F1, 2-N2, 2-N2-F1, 3-N2, 3-N2-F1, 3-N3 and 3-N3-F1) were detected as quadruply charged ions-proton adducts- at site 1 in NV5. Although triply charged ions were also observed in the averaged MS spectra (data not shown), quadruply charged ions were selected as target ions for relative quantification of the highest ionic intensity. In Figure 3*b* for site 1, 2-N2-F1 in CP4 increased in comparison to NV5. In the case of PC5, all *N*-glycans containing Fuc increased.

Concerning site 4, the spectra during 59–64 min of EIC of MS at *m/z* 1333.9–1334.9 from all samples were also averaged (averaged MS spectra not shown). The relative abundances of sialo-*N*-glycan peptides in sites 1 and 4 in all samples were calculated as described in Material and methods section and the results are shown in Figure 6. Concerning sites 2 and 3, sialo-glycopeptide (Asn203-Lsy215), which includes sites 2 and 3, was strongly detected by ESI MS (spectrum not shown). To find each distribution pattern of the *N*-glycans in site 2 and site 3, sequential digestion with endoprotease Glu-C was carried out, and glycopeptide (Asn203-Glu210, including site 2) and glycopeptide (Asn211-Lsy215, including site 3) were separated. But, unfortunately, the separated glycopeptides were barely detectable. This phenomenon may be due to overlapping of the nonglycosylated peptides.

LC-ESI MS analysis of haptoglobin asialo-glycopeptides at sites 2 and 3

To detect each glycopeptide which include sites 2 and site 3, glycopeptides from tryptic digests were enriched using affinity separation by partitioning with Sepharose CL4B, according to the method of Wada *et al.*[23] Furthermore, sialic acids were removed from the enriched glycopeptides using acidic treatment to reduce the complicated heterogeneity of the sialic acids. The samples including asialo-glycopeptides were digested with endoprotease Glu-C. In theory, digestion of asialo-glycopeptides with endoprotease Glu-C should yield (Supplemental Fig. 1): Met179-Glu194, including one *N*-glycan binding site (site 1: Asn184); Asn203-Glu210, including one *N*-glycan binding site (site 2: Asn207); Asn211-Lsy215, including one *N*-glycan binding site (site 3: Asn211); and Val236-Lsy251, including one *N*-glycan binding site (site 4: Asn241). The sample was separated by reverse-phase HPLC and the eluate was analyzed using ESI MS. The representative data shown in Figure 5*a* are the result of analysis of the serum from a normal volunteer (NV 5). Several peaks derived from glycopeptides and other peptides were detected by BPC in Figure 5*a*. Sepharose CL4B treatment reduced the peptides that interfered with ionization of the glycopeptides (compare with BPC in Fig. 3*a*). The ions detected in EIC of MSMS at *m/z* 366.3, which is the mass number of Gal-GlcNAc, indicated the presence of glycopeptides. EIC of MS scans at the mass number corresponding to the peptide of each site containing an asialo-biantennary *N*-glycan was selected to find the elution time of the glycopeptide at each site. The ion at *m/z* 1298.4–1299.4 represents $[M+2H]^{2+}$ of the glycopeptide containing site 2 with an asialo-biantennary *N*-gly-

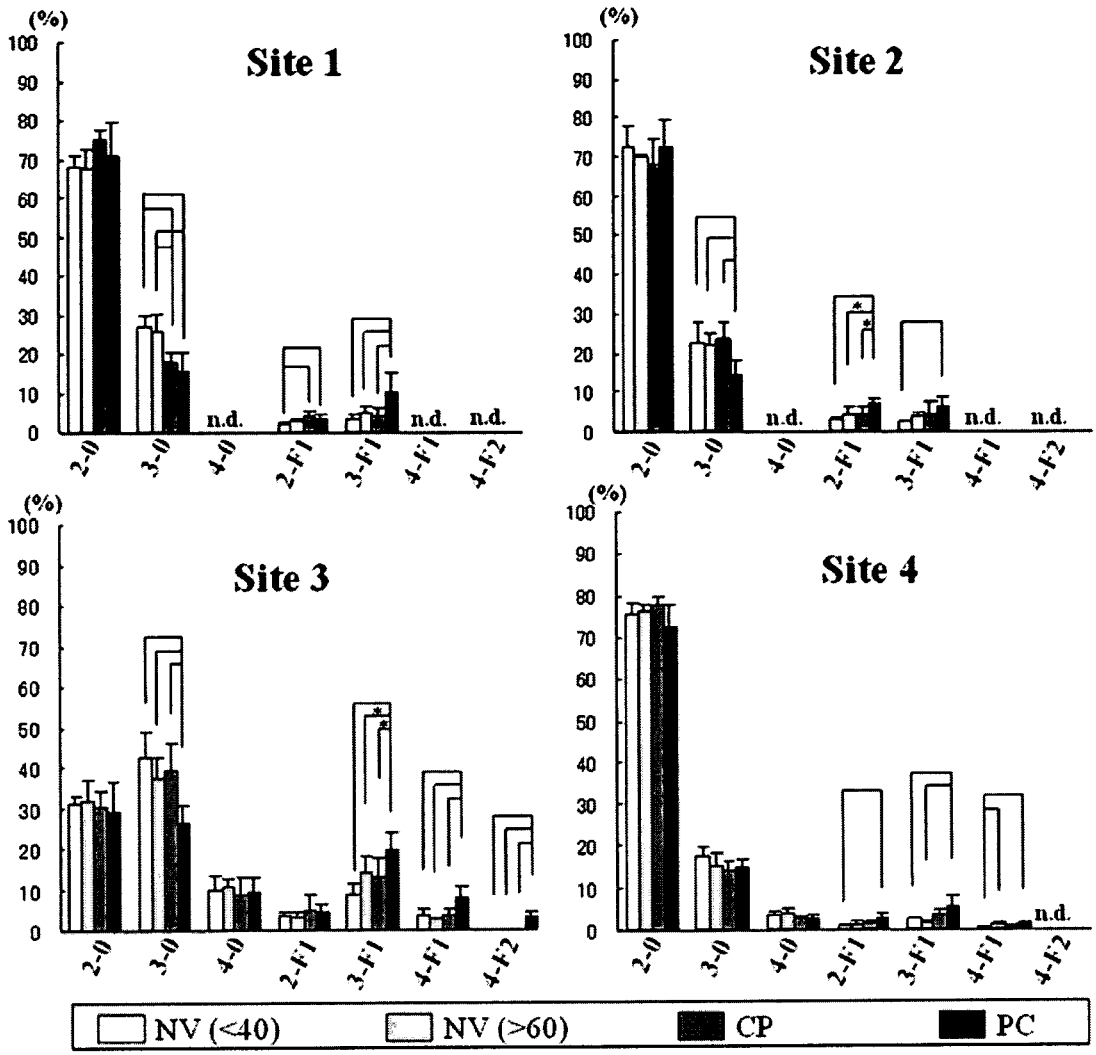

FIGURE 6 – Relative abundance (%) of glycopeptide glycoforms, including the *N*-glycan binding site of haptoglobin from sera of patients with pancreatic cancer, chronic pancreatitis and sera of old normal volunteers [over 60, NV(>60)] and young normal volunteers (under 40 NV [<40)]. The relative abundance was calculated based on the signal intensities of corresponding glycopeptides obtained from the results presented in Figures 3 and 5. The error bar represents the standard deviation (S.D.) calculated from each type of sample. The abbreviations in this figure are summarized in Figure 4. To compare 4 groups [NV (<40), NV (>60), CP and PC] nonrepeated measured ANOVA (two-tail) was used, and then each groups of two was compared by Bonferroni correction (two-tail). The annotations with asterisks in this figure indicate $p < 0.05$, and those without an asterisk indicate $p < 0.01$.

can. The ion at *m/z* 1063.8–1064.8 represents $[M+2H]^{2+}$ of the glycopeptide containing site 3 with an asialo-biantennary *N*-glycan. In the two EIC of MS, single peaks were observed at 52 (site 2) and 5 min (site 3). CP and PC samples were analyzed in the same manner as the NV samples. MS spectra during 3–7 min of EIC of MS at *m/z* 1063.8–1064.8 (site 3) were averaged; the results of NV5, CP4 and PC5 are shown in Figure 5*b*. The abbreviations for *N*-glycan structures in the glycopeptide are summarized in Figure 4. Six types of glycopeptides (2-0, 2-F1, 3-0, 3-F1, 4-0 and 4-F1) were detected as doubly charged ions-proton adducts-at site 3 in NV5. There was not much difference between CP4 and NV5. In contrast, *N*-glycans containing a Fuc (2-F1, 3-F1 and 4-F1) dramatically increased in PC5. Moreover, tetra-antennary *N*-glycans with two Fuc (4-F2) were observed only in PC samples. The results obtained from all samples are summarized in Figure 6.

Concerning site 4, observation of asialo-glycopeptides at this site was attempted. All types of *N*-glycan structures detected in the analysis of sialo-glycopeptides were observed at site 4, with the exception of the peptide having an *N*-glycan (2-F1) (data not shown). The triply charged ion for 2-F1 (*m/z* 1188.6) was hidden by a doubly charged ion derived from another unknown peptide. Therefore, the data for sialo-glycopeptides at sites 1 and 4, and for asialo-glycopeptides at sites 2 and 3 were used for comparison of relative abundance.

Identification of Lewis X structure and development of a novel tumor marker for pancreatic cancer

Average relative abundances (%) of *N*-glycans were calculated for patients with PC ($n = 5$), CP ($n = 5$), and for young NV ($n = 5$) and old normal volunteer ($n = 3$), and they were graphed with

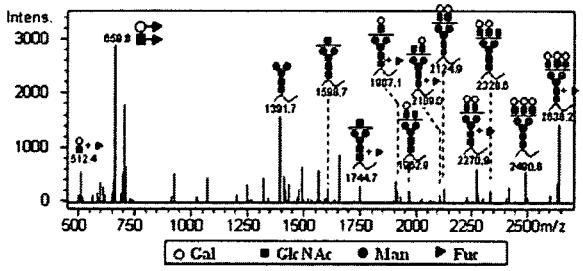

FIGURE 7 – MSMS spectrum of ion at *m/z* 1575.6 represented $[M+2H]^{+2}$ of the glycopeptide which contains site 3 with 4-F2. The data present MSMS analysis of asialo-glycopeptides derived from haptoglobin in pancreatic cancer (PC5) after digestion with trypsin and endoprotease Glu-C.

error bars representing standard deviations (Fig. 6). Site 3 was a unique *N*-glycan binding site because of the branching patterns and fucosylation. Concerning young NV samples, the relative abundances of 2-0 at sites 1–4 were 68.0%, 72.8%, 31.2% and 75.3%; the relative abundances of 3-0 at sites 1–4 were 26.8%, 22.5%, 42.8% and 17.6%. Tri-antennary *N*-glycans (3-0) were the major *N*-glycan for site 3 only, although it has been reported that the major haptoglobin *N*-glycan is bi-antennary *N*-glycan (75%).[7] Highly branched *N*-glycans (3-0 and 4-0) were abundant at site 3; therefore, fucosylated *N*-glycans (3-F1 and 4-F1) could increase at site 3.[27] The distribution of *N*-glycan structure types of at sites 1–4 were similar among PC, CP and NV. We also analyzed the *N*-glycan structures of 3 cases of old NV who were more than 60-year-old in order to match age of CP and PC samples. There was no significant difference between old NV (over 60-year-old) and young NV (under 40-year-old) except 4F-1 on site 4, although fucosylated *N*-glycans from old NV exhibited an upward trend in comparison with young NV. The relative abundance of fucosylated *N*-glycans from old NV was very similar to that from CP, because the patients with CP determined in our study were also old persons (55- to 81-year-old). In contrast, significant increases in fucosylation, such as 3-F1 on site 1, 2-F1 on site 2, 3-F1 and 4-F1 on site 3, were observed only in PC samples, compared to the others type of samples (young NV, old NV or CP). These 3-F1 on site 1 and site 3 significantly increased with a concomitant decrease in 3-0. On the basis of the results of analyses of PA-labeled *N*-glycans with α1-3/4 fucosidase and β1-4 galactosidase, the increased 3-F1 had *N*-glycans with Lewis X-type Fuc. This change was most likely due to the formation of Lewis X-type Fuc as a result of fucosyltransferase activity.

Moreover, it should be noted that tetra-antennary *N*-glycan with two Fuc (4-F2) was observed at site 3 only in PC samples (3.2%). MSMS analysis for the glycopeptide (4-F2) was performed and the result is shown in Figure 7. The fragment ion at *m/z* 659.8 represents $[M+H]^{1+}$ of Gal-GlcNAc with two Fuc residues. The structure is suggested to be the Lewis Y-type (Fucα1-2Galβ1-4GlcNAcα1-3Fuc) according to the report by Kim *et al.*[28]

Discussion

Ectopic production of haptoglobin has received attention as a novel tumor marker for several cancers.[13–15] However, most haptoglobin is produced in the liver. Glycan analysis is a promising technique to identify the organ that produces haptoglobin, because each type of fucosyltransferase is specifically expressed in each organ. Our previous study demonstrated that fucosylated haptoglobin increased in the sera of patients with PC compared to other cancer patients.[4] To be clinically useful, it is important to clarify whether fucosylated haptoglobin is increased directly by the PC or indirectly because of inflammation of the pancreas. Interestingly, the haptoglobin *N*-glycan structures at site 3 were unique compared to the structures at the other sites. While small amounts of fucosylated glycans could be detected at site 3, derived from NV and patients with CP, the 4-F2 structure was uniquely observed only in patients with PC.

In general, it has not been clarified how glycosyltransferase recognizes a specific *N*-glycan site in proteins. Several glycosyltransferases involved in branch formation, as well as fucosyltransferases, may recognize site 3 *via* unique amino acid sequences around this site or by the conformational structure of haptoglobin. The reason for increased fucosylation at site 3 in individuals with PC may be induction of glycosyltransferases in PC cells themselves or in the liver secondary to PC. Glycan changes in haptoglobin have been reported in hepatocellular carcinoma.[14,29] These changes could be caused by up-/down-regulation of glycosyltransferases in the liver and in hepatocellular carcinomas. In the case of PC, the diseased pancreas may induce a factor capable of producing fucosylated haptoglobin.[4] This hypothesis is based on the observation of fucosylated haptoglobin in the sera of patients with tumor-forming pancreatitis (data not shown). In addition, obstruction of the pancreatic duct may induce this factor, which should be identified in future studies.

To make a practical application of 4-F2 at site 3 as a tumor marker for PC, a simpler method with high throughput would be required. The procedures we used in our study might not be suitable for clinical application directly. Although ELISA systems to detect Lewis Y and/or X structures on haptoglobin are more useful, the sensitivity might not be high enough.[30] Site-specific analysis of *N*-glycans on transferrin has been incorporated into screening for congenital disorders of glycosylation (CDG) by MALDI-TOF MS in Japan.[31] Tumor marker 4-F2 at site 3 on haptoglobin could easily be detected using the same method that is used when screening for CDG. If site-specific glycan analyses of glycopeptides were possible, using crude serum samples, it would be a powerful tool as a novel glyco-marker. This analytical system is undergoing in our laboratory in next our study.

Glossary

Glycomics, an analogous term to genomics and proteomics, is the comprehensive study of glycomes, including genetic, physiologic, and other aspects. The term glycomics was formed to follow the naming convention established by genomics (which deals with genes) and proteomics (which deals with proteins). The identity of the entirety of carbohydrates in an organism is thus collectively referred to as the glycome. LC-ESI MS, a mass spectrometric ionization method based on the ionization of molecules in solution introduced from LC in an electric field at atmospheric pressure. BPC, Base Peak Chromatogram: a chromatogram in which the y-axis for each point on the chromatogram represents the intensity of the most abundant ion in the mass spectrum. EIC, Extracted Ion Chromatogram: graphical representation of the abundance of one (individual) or more (summed) selected ion(s) versus retention time.

References

1. Friess H, Kleeff J, Kulli C, Wagner M, Sawhney H, Buchler MW. The impact of different types of surgery in pancreatic cancer. Eur J Surg Oncol 1999;25:124–31.
2. Greenlee RT, Murray T, Bolden S, Wingo PA. Cancer statistics, 2000. CA Cancer J Clin 2000;50:7–33.
3. Rosty C, Goggins M. Early detection of pancreatic carcinoma. Hematol Oncol Clin North Am 2002;16:37–52.
4. Okuyama N, Ide Y, Nakano M, Nakagawa T, Yamanaka K, Moriwaki K, Murata K, Ohigashi H, Yokoyama S, Eguchi H, Ishikawa O, Ito T, et al. Fucosylated haptoglobin is a novel marker for pancreatic cancer:

a detailed analysis of the oligosaccharide structure and a possible mechanism for fucosylation. Int J Cancer 2006;118:2803–8.
5. Hakomori S. Aberrant glycosylation in tumors and tumor-associated carbohydrate antigens. Adv Cancer Res 1989;52:257–331.
6. Noda K, Miyoshi E, Gu J, Gao CX, Nakahara S, Kitada T, Honke K, Suzuki K, Yoshihara H, Yoshikawa K, Kawano K, Tonetti M, et al. Relationship between elevated FX expression and increased production of GDP-L-fucose, a common donor substrate for fucosylation in human hepatocellular carcinoma and hepatoma cell lines. Cancer Res 2003;63:6282–9.
7. Ferens-Sieczkowska M, Olczak M. Carbohydrate structures of haptoglobin in sera of healthy people and a patient with congenital disorder of glycosylation. Z Naturforsch C 2001;56:122–31.
8. He Z, Aristoteli LP, Kritharides L, Garner B. HPLC analysis of discrete haptoglobin isoform N-linked oligosaccharides following 2D-PAGE isolation. Biochem Biophys Res Commun 2006;343:496–503.
9. Goodarzi MT, Turner GA. Reproducible and sensitive determination of charged oligosaccharides from haptoglobin by PNGase F digestion and HPAEC/PAD analysis: glycan composition varies with disease. Glycoconj J 1998;15:469–75.
10. Tatsumura T, Sato H, Mori A, Komori Y, Yamamoto K, Fukatani G, Kuno S. Clinical significance of fucose level in glycoprotein fraction of serum in patients with malignant tumors. Cancer Res 1977;37:4101–3.
11. Walz G, Aruffo A, Kolanus W, Bevilacqua M, Seed B. Recognition by ELAM-1 of the sialyl-Lex determinant on myeloid and tumor cells. Science 1990;250:1132–5.
12. Zhao J, Patwa TH, Qiu W, Shedden K, Hinderer R, Misek DE, Anderson MA, Simeone DM, Lubman DM. Glycoprotein microarrays with multi-lectin detection: unique lectin binding patterns as a tool for classifying normal, chronic pancreatitis and pancreatic cancer sera. J Proteome Res 2007;6:1864–74.
13. Thompson S, Dargan E, Griffiths ID, Kelly CA, Turner GA. The glycosylation of haptoglobin in rheumatoid arthritis. Clin Chim Acta 1993;220:107–14.
14. Ang IL, Poon TC, Lai PB, Chan AT, Ngai SM, Hui AY, Johnson PJ, Sung JJ. Study of serum haptoglobin and its glycoforms in the diagnosis of hepatocellular carcinoma: a glycoproteomic approach. J Proteome Res 2006;5:2691–700.
15. Kossowska B, Ferens-Sieczkowska M, Gancarz R, Passowicz-Muszynska E, Jankowska R. Fucosylation of serum glycoproteins in lung cancer patients. Clin Chem Lab Med 2005;43:361–9.
16. Malchy B, Dixon GH. Studies on the interchain disulfides of human haptoglobins. Can J Biochem 1973;51:249–64.
17. Raugei G, Bensi G, Colantuoni V, Romano V, Santoro C, Costanzo F, Cortese R. Sequence of human haptoglobin cDNA: evidence that the α and β subunits are coded by the same mRNA. Nucleic Acids Res 1983;11:5811–19.
18. Black JA, Chan GF, Hew CL, Dixon GH. Gene action in the human haptoglobins. III. Isolation of the α-chains as single gene products. Isolation, molecular weight, and amino acid composition of α and β chains. Can J Biochem 1970;48:123–32.
19. Kurosky A, Barnett DR, Lee TH, Touchstone B, Hay RE, Arnott MS, Bowman BH, Fitch WM. Covalent structure of human haptoglobin: a serine protease homolog. Proc Natl Acad Sci USA 1980;77:3388–92.
20. Wada Y, Kadoya M. In-gel digestion with endoproteinase LysC. J Mass Spectrom 2003;38:117–18.
21. Kondo A, Suzuki J, Kuraya N, Hase S, Kato I, Ikenaka T. Improved method for fluorescence labeling of sugar chains with sialic acid residues. Agric Biol Chem 1990;54:2169–70.
22. Sano M, Hayakawa K, kato I. Purification and characterization of α-L-fucosidase from Streptomyces species. J Biol Chem 1992;267:1522–7.
23. Wada Y, Tajiri M, Yoshida S. Hydrophilic affinity isolation and MALDI multiple-stage tandem mass spectrometry of glycopeptides for glycoproteomics. Anal Chem 2004;76:6560–5.
24. Wada Y, Azadi P, Costello CE, Dell A, Dwek RA, Geyer H, Geyer R, Kakehi K, Karlsson NG, Kato K, Kawasaki N, Khoo KH, et al. Comparison of the methods for profiling glycoprotein glycans–HUPO Human Disease Glycomics/Proteome Initiative multi-institutional study. Glycobiology 2007;17:411–22.
25. Harada H, Kamei M, Tokumoto Y, Yui S, Koyama F, Kochibe N, Endo T, Kobata A. Systematic fractionation of oligosaccharides of human immunoglobulin G by serial affinity chromatography on immobilized lectin columns. Anal Biochem 1987;164:374–81.
26. Yamashita K, Kochibe N, Ohkura T, Ueda I, Kobata A. Fractionation of L-fucose-containing oligosaccharides on immobilized *Aleuria aurantia* lectin. J Biol Chem 1985;260:4688–93.
27. Schachter H, Narasimhan S, Gleeson P, Vella G. Control of branching during the biosynthesis of asparagine-linked oligosaccharides. Can J Biochem Cell Biol 1983;61:1049–66.
28. Kim YS, Itzkowitz SH, Yuan M, Chung Y, Satake K, Umeyama K, Hakomori S. Lex and Ley antigen expression in human pancreatic cancer. Cancer Res 1988;48:475–82.
29. Ekuni A, Miyoshi E, Ko JH, Noda K, Kitada T, Ihara S, Endo T, Hino A, Honke K, Taniguchi N. A glycomic approach to hepatic tumors in N-acetylglucosaminyltransferase III (GnT-III) transgenic mice induced by diethylnitrosamine (DEN): identification of haptoglobin as a target molecule of GnT-III. Free Radic Res 2002;36:827–33.
30. Manimala JC, Roach TA, Li Z, Gildersleeve JC. High-throughput carbohydrate microarray profiling of 27 antibodies demonstrates widespread specificity problems. Glycobiology 2007;17:17C–23C.
31. Wada Y. Mass spectrometry for congenital disorders of glycosylation CDG. J Chromatogr B Analyt Technol Biomed Life Sci 2006;838:3–8.

Glycobiology vol. 17 no. 5 pp. 455–466, 2007
doi:10.1093/glycob/cwl079
Advance Access publication on December 15, 2006

Crystal structure of mammalian α1,6-fucosyltransferase, FUT8

Hideyuki Ihara[2], Yoshitaka Ikeda[3,4], Sachiko Toma[5,6], Xiangchun Wang[2,7], Tadashi Suzuki[7], Jianguo Gu[7,8], Eiji Miyoshi[7], Tomitake Tsukihara[6], Koichi Honke[4,9], Akio Matsumoto[2], Atsushi Nakagawa[6], and Naoyuki Taniguchi[1,2]

[2]Department of Disease Glycomics, Research Institute for Microbial Diseases, Osaka University, Taniguchi Research Group, 4th Floor, Center for Advanced Science & Innovation, Osaka University, 2-1, Yamadaoka Suita, Osaka 565-0871, Japan; [3]Division of Molecular Cell Biology, Department of Biomolecular, Sciences, Saga University Medical School, 5-1-1 Nabeshima, Saga 849-8501, Japan; [4]Core Research for Evolution Science and Technology (CREST), Japanease Science and Technology Agency (JST), 4-1-8, Honcho, Kawaguchi-shi, Saitama 332-0012, Japan; [5]Graduate School of Pharmaceutical Sciences, University of Tokyo, Hongo 7-3-1, Tokyo, Bunkyo-ku, 113-0033, Japan; [6]Institute for Protein Research, Osaka University, 3-2 Yamadaoka, Suita, Osaka 565-0871, Japan; [7]Department of Biochemistry, Osaka University Graduate School of Medicine, B1, 2-2 Yamadaoka, Suita, Osaka 565-0871, Japan; [8]Division of Regulatory Glycobiology, Institute of Molecular Biomembrane and Glycobiology, Tohoku Pharmaceutical University, 4-4-1 Komatsushima, Aoba-ku, Sendai, Miyagi 981-8558, Japan; and [9]Department of Molecular Genetics, Kochi University Medical School, Kohasu, Oko-cho, Nankoku, Kochi 783-8505, Japan

Received on October 30, 2006; revised on November 30, 2006; accepted on December 1, 2006

Mammalian α1,6-fucosyltransferase (FUT8) catalyses the transfer of a fucose residue from a donor substrate, guanosine 5′-diphosphate-β-L-fucose to the reducing terminal *N*-acetylglucosamine (GlcNAc) of the core structure of an asparagine-linked oligosaccharide. α1,6-Fucosylation, also referred to as core fucosylation, plays an essential role in various pathophysiological events. Our group reported that FUT8 null mice showed severe growth retardation and emphysema-like lung-destruction as a result of the dysfunction of epidermal growth factor and transforming growth factor-β receptors. To elucidate the molecular basis of FUT8 with respect to pathophysiology, the crystal structure of human FUT8 was determined at 2.6 Å resolution. The overall structure of FUT8 was found to consist of three domains: an N-terminal coiled-coil domain, a catalytic domain, and a C-terminal SH3 domain. The catalytic region appears to be similar to GT-B glycosyltransferases rather than GT-A. The C-terminal part of the catalytic domain of FUT8 includes a Rossmann fold with three regions that are conserved in α1,6-, α1,2-, and protein *O*-fucosyltransferases. The SH3 domain of FUT8 is similar to other SH3 domain-containing proteins, although the significance of this domain remains to be elucidated. The present findings of FUT8 suggest that the conserved residues in the three conserved regions participate in the Rossmann fold and act as the donor binding site, or in catalysis, thus playing key roles in the fucose-transferring reaction.

Key words: fucosyltransferase/core fucosylation/*N*-glycan/crystal structure/glycosyltransferase

Introduction

The fucosylation of glycoconjugates in mammalian organisms is related to a wide variety of biological processes, including cell adhesion, blood antigens, and some severe diseases including cancer metastasis, congenital disorders of glycosylation, and various microbial and virus infections (Staudacher et al. 1999; Becker and Lowe 2003). Fucosylation via α1,2-, α1,3-, α1,4-, α1,6-linkages, and protein *O*-fucosylation are accomplished by the action of specific individual fucosyltransferases (Staudacher et al. 1999; Oriol and Mollicone 2002; Miyoshi and Taniguchi 2002; Becker and Lowe 2003). Asparagine-linked oligosaccharides (*N*-glycans) of glycoproteins are ubiquitously α1,6-fucosylated (Miyoshi et al. 1997; Miyoshi, Noda, Yamaguchi et al. 1999). α1,6-Fucosylation, also known as core fucosylation, is frequently observed in *N*-glycans of α-fetoprotein, a well-known tumor marker for hepatocellular carcinoma but not for chronic liver disease (Taketa et al. 1993; Noda et al. 1998). To elucidate the biological functions associated with core fucosylation, overexpression experiments with mammalian α1,6-fucosyltransferase (FUT8), which is an eukaryotic α1,6-fucosyltransferase, and a key enzyme in core fucosylation synthesis, were performed. The findings showed that experimental cancer metastasis is suppressed by the core fucosylation of α5β1 integrin (Miyoshi, Noda, Ko et al. 1999). Moreover, the core fucosylation of *N*-glycans in human immunoglobulin (Ig) G1 was found to regulate antibody-dependent cellular cytotoxicity (ADCC) (Shields et al. 2002; Shinkawa et al. 2003). The lack of core fucose on the IgG1 molecule results in an enhancement in ADCC activity of up to 100-fold, suggesting that this core fucose-deficient IgG1 would be useful in terms of antibody therapy in cancer treatment. In addition, it has been directly verified that α1,6-fucosylation regulates the function of immunoglobulin by modifying its physicochemical characteristics (Okazaki et al. 2004). Very recently, our group reported that disruption of the *FUT8* gene in mice leads to phenotypes of growth retardation, lung emphysema, and death during postnatal development (Wang et al. 2005). These severe phenotypes were found to be mainly due to the lack of core fucosylation of epidermal growth factor, transforming growth factor-β receptors (Wang et al. 2005, 2006; Taniguchi et al. 2006), and other molecules (Lee et al. 2006; Li et al. 2006; Zhao et al. 2006). These studies strongly suggest that FUT8 and its enzymatic product, a core fucose play pivotal roles in a variety of physiological and pathophysiological events.

[1]To whom correspondence should be addressed; e-mail: tani52@wd5.so-net.ne.jp

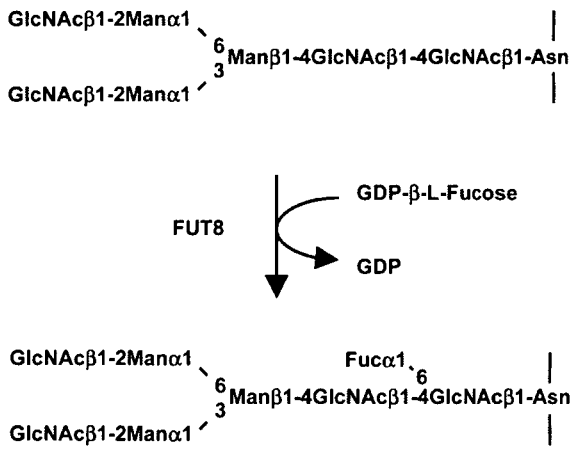

Fig. 1. Reaction catalyzed by FUT8. FUT8 transfers a fucose residue from GDP-β-L-fucose to the innermost GlcNAc of an Asn-linked oligosaccharide.

FUT8 catalyzes the transfer of a fucose residue from the donor substrate, GDP-β-L-fucose, to the innermost *N*-Acetylglucosamine (GlcNAc) residue in *N*-glycans via α1,6-linkage with inversion of the anomeric center of the transferred fucose (Figure 1) (Wilson et al. 1976). FUT8 is known to be a typical type II membrane protein and is localized in the Golgi apparatus, along with many other glycosyltransferases (Uozumi, Yanagidani et al. 1996), and is also known to be abundant especially in brain tissue (Nakakita et al. 1999). FUT8 has been extensively studied with respect to its substrate specificity (Longmore and Schachter 1982; Voynow et al. 1991; Kaminska et al. 1998; Paschinger et al. 2005; Ihara et al. 2006). As indicated in earlier studies, FUT8 requires at least two structural features in oligosaccharide acceptors: (a) β1,2-GlcNAc residue linked to the α1,3-mannose arm in the tri-mannose core structure of *N*-glycans (Longmore and Schachter 1982; Voynow et al. 1991; Kaminska et al. 1998; Paschinger et al. 2005) and (b) β-linkage between the reducing terminal GlcNAc and the asparagine residue in the *N*-glycosylation consensus sequence (Voynow et al. 1991). In addition, the reaction of FUT8 with the substrate is prevented by the presence of the bisecting GlcNAc, which is produced by the action of β1,4-*N*-acetylglucosaminylytransferase (GnT-III) (Longmore and Schachter 1982), and also by α1,3-fucose at the reducing terminal GlcNAc residue, as observed in insects (Staudacher and Marz 1998; Paschinger et al. 2005). Regarding donor substrate specificity, on the other hand, our recent study indicated that FUT8 strongly recognizes the base portion and diphosphoryl group of GDP, a part of the donor substrate (Ihara et al. 2006). As reported previously (Breton et al. 1998; Oriol et al. 1999; Takahashi et al. 2000; Martinez-Duncker et al. 2003; Okajima et al. 2005), three small regions that are highly conserved among α1,2-, α1,6-, and protein *O*-fucosyltransferases appear to participate in the possible binding site for GDP-β-L-fucose. Furthermore, site-directed mutagenesis studies indicated that two arginine residues in one of the conserved regions, Arg-365 and 366 in human FUT8 play important roles in donor binding (Takahashi et al. 2000). In kinetic analyses, it was found that the reaction of FUT8 follows a rapid equilibrium random mechanism (Ihara et al. 2006). However, the catalytic mechanism for this enzyme is not known in detail, and the molecular and chemical bases for the catalysis remains to be investigated.

In the present study, we solved the overall structure of human FUT8 at 2.6 Å resolution, in order to more understand the molecular basis for the action of FUT8. The results showed that FUT8 is comprised of three domains, an N-terminal coiled-coil domain, a catalytic domain, and a C-terminal SH3 domain. The C-terminal part of the catalytic domain of FUT8 includes a Rossmann fold with three conserved regions in α1,6-, α1,2-, and protein *O*-fucosyltransferases. Furthermore, site-directed mutagenesis experiment showed that several residues, which are all highly conserved in the three fucosyltransferases in this fold are essential for the enzyme activity of FUT8.

Results and discussion

Overall structure of FUT8

The recombinant human FUT8 used in the structural analysis was designed to express a soluble form by the truncating transmembrane and stem regions, as described previously (Ihara et al. 2006). The expressed protein corresponds to residues 68–575 and contained some additional amino acids. We used this recombinant protein for the crystallographic analysis, and succeeded in solving its structure at 2.6 Å resolution. As illustrated in Figure 2, the residues of Leu-108 to Glu-572 are modeled, however, the N-terminus (residues 68–107), C-terminus (residues 573–575), and the residues 368–372 are disordered in this structure. The overall structure of FUT8 is comprised of 15 strands and 16 helices (Figures 2 and 3). Several distinct features are observed in the structure of FUT8 (Figure 2). (a) At the N-terminus of FUT8, two long antiparallel α-helices (residues 109–173, α1 and α2 helices) form a coiled-coil structure. (b) The putative catalytic domain is comprised of two structures, an open sheet α/β structure and a Rossmann fold which is frequently found in nucleotide binding proteins including glycosyltransferases. The former structure contains five helices and three β-strands (residues 203–297, α4 and 3H1–3 helices, and β1-3 strands), and is at the N-terminal side of the catalytic domain of FUT8. The latter Rossmann fold contains five helices and five β-strands (residues 359–492, α8–11 and 3H5 helices, and β5–9 strands), and is at C-terminal side of the catalytic domain of FUT8. These two structures are linked via three helices, the α5, α6, and α7 helices. (c) The SH3 domain, which has been reported in various types of cytosolic proteins, is located at the C-terminus of FUT8.

In order to compare the fold of FUT8 with known structures, each part of the FUT8 structure was applied to database searching (DALI server) (Holm and Sander 1993). As summarized in Table I, the matching proteins are human lysine-specific demethylase-1 (Stavropoulos et al. 2006) to the coiled-coil structure of FUT8 (residues 108–174), ATP-binding hypothetical protein (Zarembinski et al. 1998) to the catalytic region of FUT8 (residues 201–500), *Escherichia coli* ADP-heptose lps heptosyltransferase II (PDB No., 1PSW), which belongs to the GT-B glycosyltransferase group, to the Rossmann fold (residues 348–500), *E. coli* carbamoyl phosphate synthetase (Thoden et al. 1999) to the open sheet α/β structure (residues 201–300) of the N-terminal region of the catalytic domain.

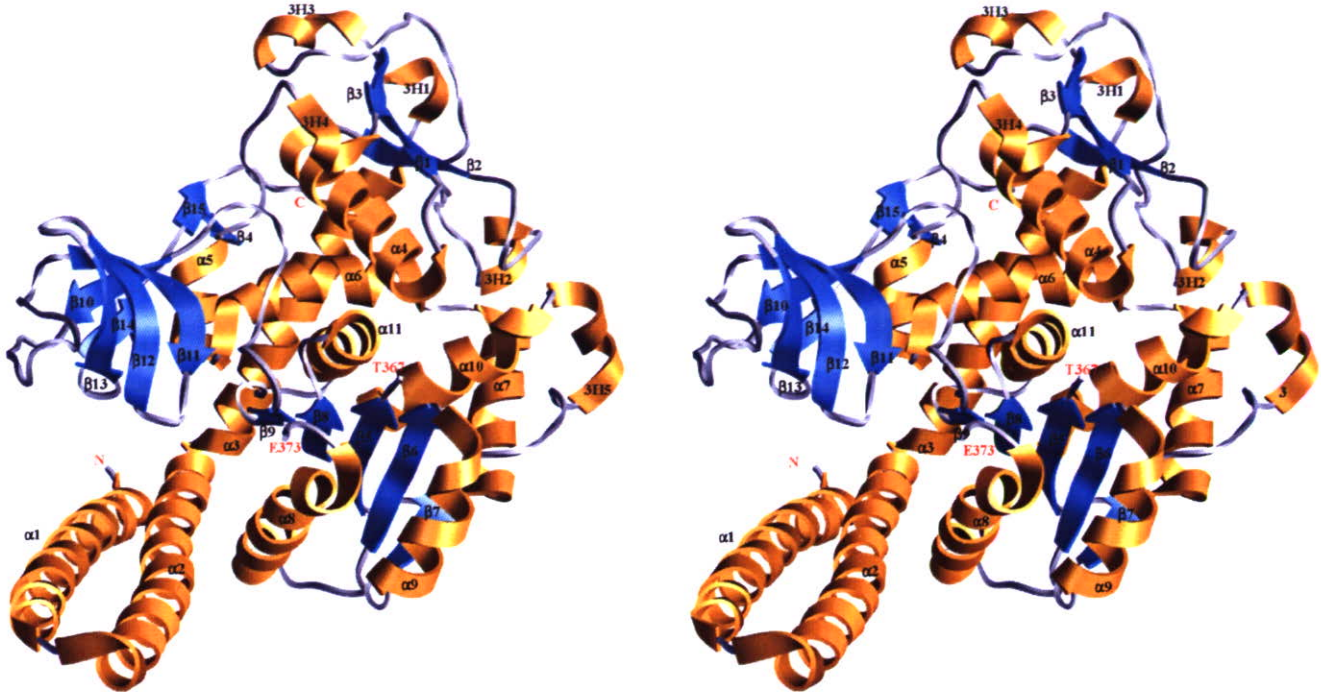

Fig. 2. Overall structure of human FUT8. Stereo view of the overall structure of the catalytic region of FUT8 (PDB No. 2DE0) is indicated by a ribbon diagram. The secondary structures are highlighted, and helices and β-strands are shown in orange and blue, respectively. Thr-367 and Glu-373 colored in red means that the residues, Asp-368 to Thr-372 are disordered. All figures in this study were produced using the program, UCSF Chimera (Pettersen et al. 2004).

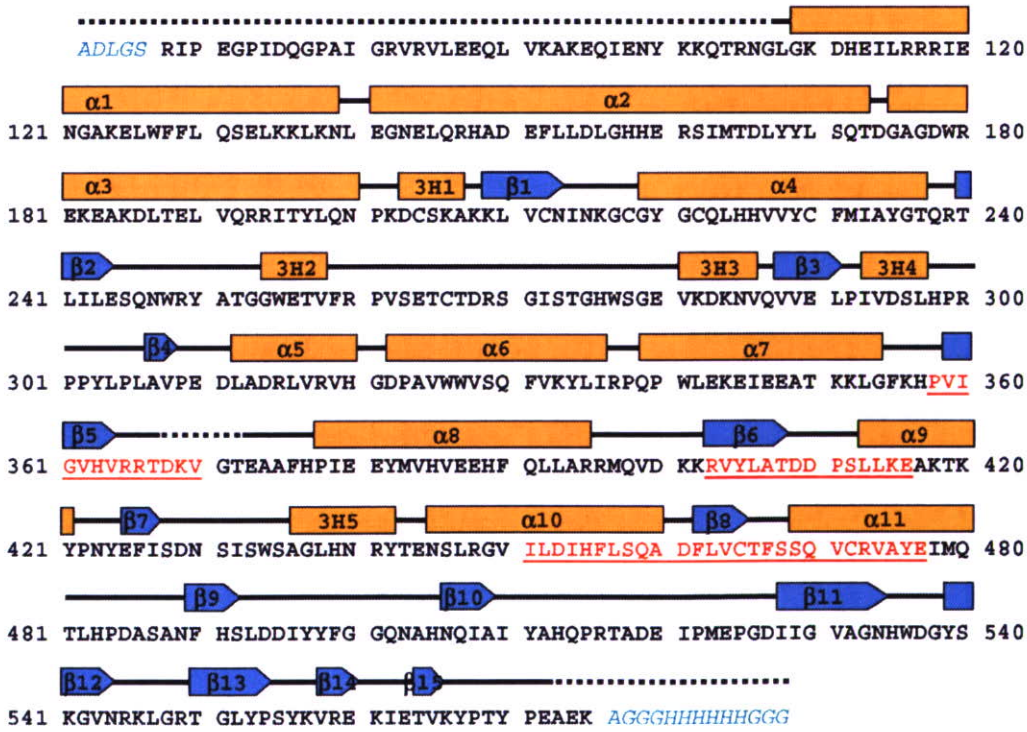

Fig. 3. The amino acid sequence and secondary structure of human FUT8. Amino acid residues 68–575 that were examined by structural analysis are shown. Residues 358–370, 403–416, and 451–477, underlined and in red, indicate the three conserved regions among the α1,2-, α1,6-, and protein *O*-fucosyltransferases, as shown in Figure 5A. As illustrated in the diagram of the secondary structures above the sequence, the cylinder and arrow denote the helix and β-strand, respectively. Some residues indicated in light blue and italic are additional residues for recombinant expression at the N- and C-terminus. The dashed line denotes regions that are disordered in the structural analysis (residues 68–117, 368–372, and 573–575). Helices, α1 – 11, are α-helices and 3H1–4 mean 3_{10}-helices.

Table I. Structural similarities of FUT8 to other proteins

Applied query of FUT8 (residues)	Protein	PDB	*Z* score	Root mean square deviation
Coiled-coil region (residues 108–174)	Human lysine-specific demethylase-1	2H94	8.3	2.0
Open sheet α/β structure (residues 201–300)	*E. coli* carbamoyl phosphate synthetase	1C3O	3.6	3.3
Rossmann fold (residues 348–500)	ADP-heptose lipopolysaccharide heptosyltransferase II	1PSW	6.1	3.0
Catalytic region (residues 201–500)	ATP-binding hypothetical protein	1MJH	6.0	3.0
	Gtfb, β-glucosyltransferase	1IIR	5.2	3.3
	Trehalose-6-phosphate synthase	1GZ5	5.1	3.9
	Sialyltransferase from *Pasteurella multocida*	2EX0	5.0	3.3
SH3 domain (residues 502–562)	Yeast actin binding protein	1JO8	11.0	1.3
	Neutrophil cytosol factor 4	1W6X	11.0	1.2
	c-Crk, oncogene protein	1CKA	10.3	1.4
	p56 Lck, the Src family kinase	1LCK	11.6	1.1

The SH3 domain (residues 502–562) of FUT8 has relatively high similarities to that of many proteins, and will be described in detail in the section *Src homology 3 domain of FUT8*. These results indicate that some parts of FUT8, the coiled-coil structure, the Rossmann fold, and the SH3 domain have structural similarities to some proteins, however, the overall structure of FUT8 has low similarities to any currently known proteins.

Comparison to other known glycosyltransferase structures

The structures of several glycosyltransferases have been solved by crystallographic analysis to date, and are classified into two structural superfamilies, GT-A and GT-B (Couinho et al. 2003; Qasba et al. 2005). GT-A enzymes have a specific motif, the DXD or EXD motif, which is required for metal ion and donor substrate interaction. The folds of these enzymes contain a Rossmann fold of two tightly associated domains at the N-terminal. The mixed β-sheets, which functions as the acceptor-binding domain are also located at the C-terminal (Couinho et al. 2003; Qasba et al. 2005). On the other hand, GT-B enzymes have folds consisting of two similar Rossmann folds (Couinho et al. 2003; Qasba et al. 2005). It is known that the Rossmann fold in many proteins is a nucleotide or nucleotide-sugar binding domain. In fact, several glycosyltransferases, whose structures have been solved, were shown to bind the nucleotide sugar to the Rossmann fold regardless of whether a metal ion is required for activity (Qasba et al. 2005).

Our structural study reveals that the structure of FUT8 contains one Rossmann fold, similar to GT-A enzymes (Figure 2). However, the results of database searching retrieved GT-B enzymes from the database when the catalytic region (residues 201–500) of FUT8 was used as a search query. Retrieved GT-B enzymes with a *Z* score of not <5, were ADP-heptose lipopolysaccharide heptosyltransferase II (PDB No., 1PSW) and Gtfb, β-glucosyltransferase (Mulichak et al. 2001), trehalose-6-phosphate synthase (Gibson et al. 2002), and sialyltransferase from *Pasteurella multocida* (Ni et al. 2006) (Table II). These enzymes were found to be similar to only the Rossmann fold part of FUT8. However, the overall shape of the catalytic region of FUT8 seems to be like that of GT-B enzymes (Figure 4). At the same time, the catalytic region of FUT8 was compared with some GT-A glycosyltransferases, CstII, sialyltransferase from *Campylobacter jejuni* (Chiu et al. 2004), yeast α1,2-mannosyltransferase (Lovsanov et al. 2004), mannosylglycerate synthase from *Rhodothermus marinus* (Flint et al. 2005), and leukocyte type core2 β1,6-*N*-acetylglucosaminyltransferase (Pak et al. 2006). Leukocyte type core2 β1,6-*N*-acetylglucosaminyltransferase belongs to the GT-A enzyme family, and is a metal-independent glycosyltransferase without a DXD motif (Pak et al. 2006). Yeast α1,2-mannosyltransferase and mannosylglycerate synthase from *Rhodothermus marinus*, which are also GT-A enzymes, are known to utilize a GDP–sugar as the donor substrate for enzyme reaction like FUT8. CstII is classified as a GT-A enzyme, because this enzyme contains a single Rossmann fold. However, the connectivity of secondary structure and the lack of a DXD motif in this enzyme are different from typical GT-A enzymes (Chiu et al. 2004). The catalytic region of FUT8 was observed to have no or little similarity to these GT-A enzymes (mannosylglycerate synthase, *Z* score 2.7; CstII, 1.2; α1,2-mannosyltransferase, 1.6; and core2 β1,6-*N*-acetylglucosaminyltransferase, 2.0). These results support that the catalytic region of FUT8 is likely to be closer to GT-B than GT-A enzymes, although the structure of the N-terminal part of the catalytic region of FUT8 is not to be a typical Rossmann fold. In addition, FUT8 does not contain a DXD motif and is fully active without a metal ion. These properties of FUT8 are also similar to those of GT-B than GT-A enzymes.

Putative catalytic region of FUT8

For glycosyltransferases like nucleotide-binding proteins, it has been reported that the flexible loop which is essential for their enzymatic reactions is located in close proximity to the nucleotide-sugar binding site (Qasba et al. 2005). This flexible loop was determined in the structures of β1,4-galactosyltransferase I, which is one of the most extensively investigated glycosyltransferases by structural analyses involving the donor substrate-complexed form, as well as the unliganded form (Gastinel et al. 1999; Ramasamy et al. 2003; Ramakrishnan et al. 2004). By contrast, in several enzymes, for example, blood group A- and B-transferases, β1,3-glucuronyltransferases, and β-glucosyltransferase, the flexible loop could not be determined in the structure of the ligand-free

Table II. Data collection and refinement statistics for the structure of FUT8

Data set	Native2	Pt derivative
Data collection		
Space group	$P6_522$	$P6_522$
Wavelength (Å)	0.9	0.9
Unit cell		
a (Å)	90.0	90.6
b (Å)	90.0	90.6
c (Å)	380.7	380.6
Resolution	50–2.6 (2.69–2.60)	50–3.0 (3.11–3.00)
Number of unique reflections	28706	19663
Completeness (%)	97.7 (80.2)	99.9 (99.8)
R_{merge} (%)[b]	5.7 (39.5)	9.2 (68.6)
$I/\sigma(I)$	16.1 (1.4)	11.39 (1.34)
Phase determination		
R_{Cullis} (acentric/centric, isomorphous)[c]	0.86/0.85	
R_{Cullis} (anomalous)[c]	0.98	
Phasing power (acentric/centric)[d]	0.81/0.78	
Number of heavy atom sites		1
Mean overall figure of merit (after DM[e])	0.83	
Refinement		
Resolution (Å)	50–2.61	
R_{work} (%)[f]	22.0	
R_{free} (%)[g]	28.3	
Root mean square deviation		
Bond length (Å)	0.017	
Bond angle (°)	1.75	
Ramachandran plot		
Most favored (%)	88.1	
Additional allowed (%)	11.4	
Generously allowed (%)	0.5	

[a]The number in parentheses represents statistics in the highest resolution shell.
[b]$R_{merge} = \Sigma|I - <I>|/\Sigma < I>$, where I is the observed intensity, and $<I>$ is the averaging intensity of multiple symmetry-related observations of that reflection.
[c]$R_{Cullis} = \Sigma\varepsilon/\Sigma|F_{PH}-F_P|$, where ε = phase-integrated lack of closure.
[d]Phasing Power = $<|F_{Hcalc}|/\varepsilon,>$, where ε = phase-integrated lack of closure.
[e]DM means density modification performed with SOLOMON and DM implemented in SHARP.
[f]$R_{work} = \Sigma||F_{obs}|$ − $|F_{calc}||/\Sigma|F_{obs}|$, where F_{obs} and F_{calc} are the observed and calculated structure factors for data used for refinement, respectively.
[g]$R_{free} = \Sigma||F_{obs}|$− $|F_{calc}||/\Sigma|F_{obs}|$ for 5% of the data not used at any stage of the structural refinement.

form and/or donor substrate-bound form (Pedersen et al. 2000; Unligil et al. 2000; Gastinel et al. 2001; Mulichak et al. 2001; Patenaude et al. 2002; Pedersen et al. 2003; Kakuda et al. 2004). In the case of FUT8, the region consisting of residues 368–372 is disordered probably due to its flexibility (Figures 2 and 3), and it seems likely that the region corresponds to a flexible loop. This flexible loop is located in the Rossmann fold of the FUT8 structure, as has been found in other glycosyltransferases (Figures 2 and 3), and thus it is likely that this loop plays an important role in the catalytic mechanism of FUT8.

It has been previously reported that three short regions are highly conserved in the amino acid sequences of FUT8, α1,2-fucosyltransferase related to H-antigen synthesis, NodZ, which is a bacterial α1,6-fucosyltransferase and modifies the Nod factor related to plant root nodulation, and protein *O*-fucosyltransferase, which is involved in Notch signaling (Breton et al. 1998; Oriol et al. 1999; Takahashi et al. 2000; Martinez-Duncker et al. 2003; Okajima et al. 2005). As indicated in our previous study involving site-directed mutagenesis and kinetic analysis, two arginine residues (Arg-365 and 366 of human FUT8) in one of the conserved regions play important roles in the binding of GDP-β-L-fucose (Takahashi et al. 2000). Recently, another group also reported similar roles for the equivalent arginine residues in the *O*-fucosyltransferase (Okajima et al. 2005). Our current study of the structure of FUT8 shows that three conserved regions are located adjacently to one another and are located within the Rossmann fold of FUT8 (Figure 3). These results strongly suggest that the three conserved regions and the flexible loop of FUT8 are functional in fucose-transferring reactions.

Site-directed mutagenesis

Structural analyses of the complex forms with the substrates are desired to better elucidate the catalytic mechanism of the α1,6-fucose transfer reaction. Despite much effort, such an analysis has not yet been successful for FUT8. Therefore, site-directed mutagenesis experiment was performed to determine roles for amino acid residues in or around Rossmann fold which is presumably the active site of FUT8. Eight amino acid residues, Asp-368, Lys-369, Glu-373, Tyr-382, Asp-409, Asp-410, Asp-453, and Ser-469 of human FUT8 were selected to be mutagenized because, in addition to their location, these residues are perfectly conserved among various species, vertebrates, insect, nematode, and ascidian (Figure 5A). As shown by the structural analysis of FUT8 in this study (Figure 5B), these selected residues were found to be located in the proximity of Arg-365 which is known to be the essential residue for its activity, as reported previously (Takahashi et al. 2000). These residues are also highly conserved in the motif conserved among other fucosyltransferases, α1,2-, and protein *O*-fucosyltransferase (Martinez-Duncker et al. 2003), as shown in motifs I, II, and III of Figure 5A, and those requirements expected from the alignment are consistent with the suggestion by the present structural analysis.

The mutant enzymes, in which the residues to be examined are replaced by alanine, were expressed in COS-1 cells, and were investigated by sodium dodecyl sulfate–polyacrylamide gel electrophoresis (SDS–PAGE) and FUT8 enzyme activity assay (Figure 5C and D). As indicated by a western blot analysis, the expression levels of these mutants were similar to that of the wild-type enzyme (Figure 5C). In the activity assay, however, it was found that D368A, K369A, E373A, Y382A, D409A, D453A, and S469A mutants were inactive because the level of enzyme activities in the transfected COS-1 cells were as low as that of the parental COS-1 cell, vector-transfected cell and the R365A mutant, which is

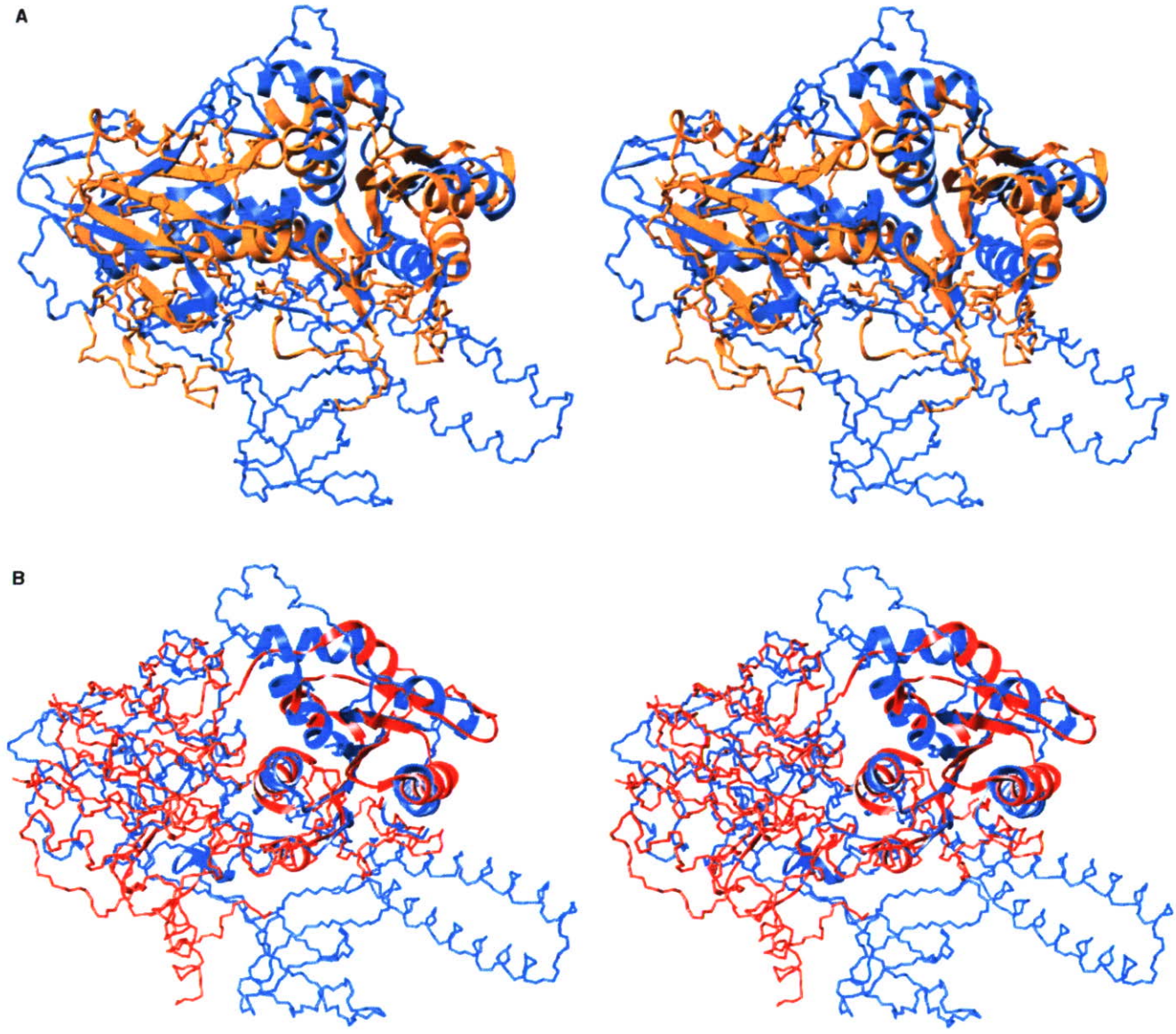

Fig. 4. Overlapping of GT-B glycosyltransferase on FUT8.Two GT-B glycosyltransferases, in which the Rossmann fold is similar to that of FUT8, were overlapped on FUT8. The main-chains of the enzymes are indicated. Regions with similarities are shown as a ribbon model. ADP-heptose lps heptosyltransferase II (**A**, PDB No. 1PSW) and Gtfb, β-glucosyltransferase (**B**, PDB No. 1IIR) are indicated in orange and red, respectively. FUT8 is indicated in blue.

known as the inactive mutant (Takahashi et al. 2000) (Figure 5D). The D410A mutant was found to be fully active, similar to the wild-type enzyme, suggesting that Asp-410 is not required for enzyme activity despite its location. It appears that Asp-368, Lys-369, Glu-373, Tyr-382, Asp-409, Asp-453, and Ser-469 play essential roles in the activity of FUT8 and are involved in the catalytic mechanism.

Asp-453 of human FUT8 as well as Arg-365 appears to be perfectly conserved among α1,2-, α1,6-, and *O*-fucosyltransferases (Martinez-Duncker et al. 2003), as shown in motifs I and III of Figure 5A. Consistent with the requirement of Asp-453 in FUT8, the equivalent Asp residue of NodZ is also essential for enzymatic activity (Chazalet et al. 2001). These results strongly suggest that Asp-453 and its equivalents serve a common function in α1,2-, α1,6-, and *O*-fucosyltransferases, possibly as a critical catalytic residue. Another essential aspartic residue, Asp-409 is located near Arg-365 and arranged face-to-face with Asp-453 (Figure 5B and D), and thus it seems more likely that a pair of Asp-409 and Asp-453 play a critical role as a general acid–base catalyst in the catalytic mechanism, as expected in inverting glycosidases and glycosyltransferases (White and Rose 1997; Unligil and Rini 2000; Tarbouriech et al. 2001; Zechel and Withers 2001). Such pairs of the residues have not yet been observed in the crystal structures of inverting glycosyltransferases.

On the other hand, Asp-368 and Lys-369, the locations of which were not determined but would be expected to be

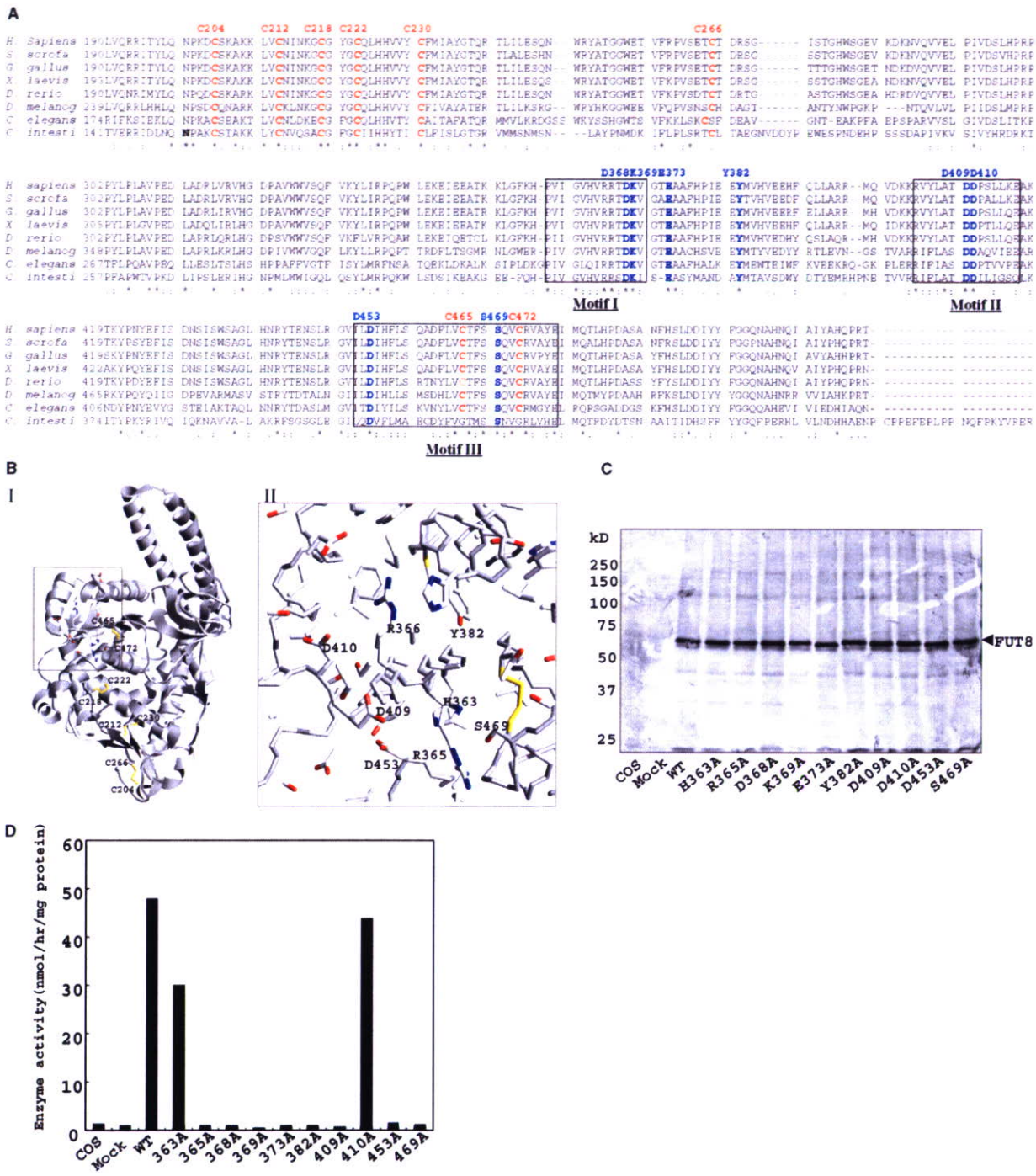

Fig. 5. Site-directed mutagenesis of the conserved amino acid residues of FUT8. (**A**) An alignment analysis of the catalytic regions of FUT8 from several species was carried out using CLUSTAL W. The amino acid residues which are conserved in all species are highlighted in bold. The conserved cysteine residues are indicated in red, and mutated residues are indicated in blue. The motif I (residues 358–370), motif II (residues 403–416), and motif III (451–477), which are conserved in three fucosyltransferases, α1,2-, α1,6-, and protein O-fucosyltransferases, are indicated in a box. GenBank accession numbers for FUT8 are: *Homo sapiens*, BAA19764; *Mus musculus*, NP_058589; *Sus scrofa*, BAA13157; *Gallus gallus*, CAH25853; *Xenopus laevis*, AAH79978; Danio *rerio*, CAH03675; *Drosophila melanogaster*, AAF48079; *C. elegans*, AAN84870; and *Ciona intestinalis*, CAD561622. (**B**) (I) The overall structure is shown as a ribbon model. Locations of the mutated residues near Arg-365 of FUT8 are indicated in a box. Side chains of the mutated residues are shown by stick. Conserved disulfide bonds are indicated in yellow. (II) The region around Arg-365 in box of Figure 5B-I is closed up. His-363, Arg-365, and Arg-366 were examined, as reported previously (Takahashi et al. 2000). The σ_A weighted $2F_o - F_c$ map contoured at 1 is also indicated. (**C**) The wild-type and mutant enzymes were transiently expressed in COS-1 cells. Cell lysates were separated on 8% SDS-gels and analyzed by immunoblot using anti-(FUT8) IgG. COS and mock indicate nontransfected and vector-transfected COS-1 cells, respectively. H363A and R365A are the controlled mutants. (**D**) Enzyme activities of FUT8 and its mutants were assayed using Asn-linked oligosaccharide acceptor labeled with *N*-[2-(2-pyridylamino)ethyl]-succinamic acid 5-norbornene-2,3-dicarboxyimide ester, as described in *Materials and methods*.

within the flexible loop of FUT8, were found to be essential for enzyme activity (Figure 5D). These results suggest that the flexible loop of FUT8, containing Asp-368 and Lys-369, plays an important role in the function of the enzyme.

Conserved disulphide bonds of FUT8 in vertebrate and invertebrate

Human FUT8 contains eight cysteine residues (Cys-204, 212, 218, 222, 230, 266, 465, and 472) (Yanagidani et al. 1997). This study identified all combinations of cysteines that form four disulfide bonds (Cys204–266, 212–230, 218–222, and 465–472 of human FUT8). Five cysteine residues (Cys-204, 212, 218, 222, and 230) of human FUT8 are perfectly conserved among vertebrates, insect, nematode, and ascidian (Figure 5A and B). Cys-266 of human FUT8 is predominantly conserved except in *Chlostridium elegans*, although in the *C. elegans* enzyme, the amino acid residue equivalent to Cys-266 of human FUT8 is replaced by serine (Ser-252 in *C. elegans*), the neighboring Cys-251 in *C. elegans* appears to be the substitute for the conserved cysteine residue (Figure 5A). Cys-465 and 472 are conserved in vertebrates, insect, and nematode, but not in asidian (Figure 5A). Because it has been reported that human FUT8 is sensitive to reducing condition (Yanagidani et al. 1997; Kaminska et al. 1998; Kaminska et al. 2003), some of the four disulfide bonds of FUT8 which are strongly conserved may play important roles in the correct folding of the protein and/or its stability rather than for the enzymatic function of catalysis.

Src homology 3 domain of FUT8

Early studies reported that the amino acid sequence of FUT8 is similar to some proteins that contain an SH3 domain (Javaud et al. 2000, 2003). The structural analysis confirms that the SH3 domain is actually folded at the C-terminus of FUT8 (Figures 2 and 6). By searching the DALI database, some other proteins were identified from the database as

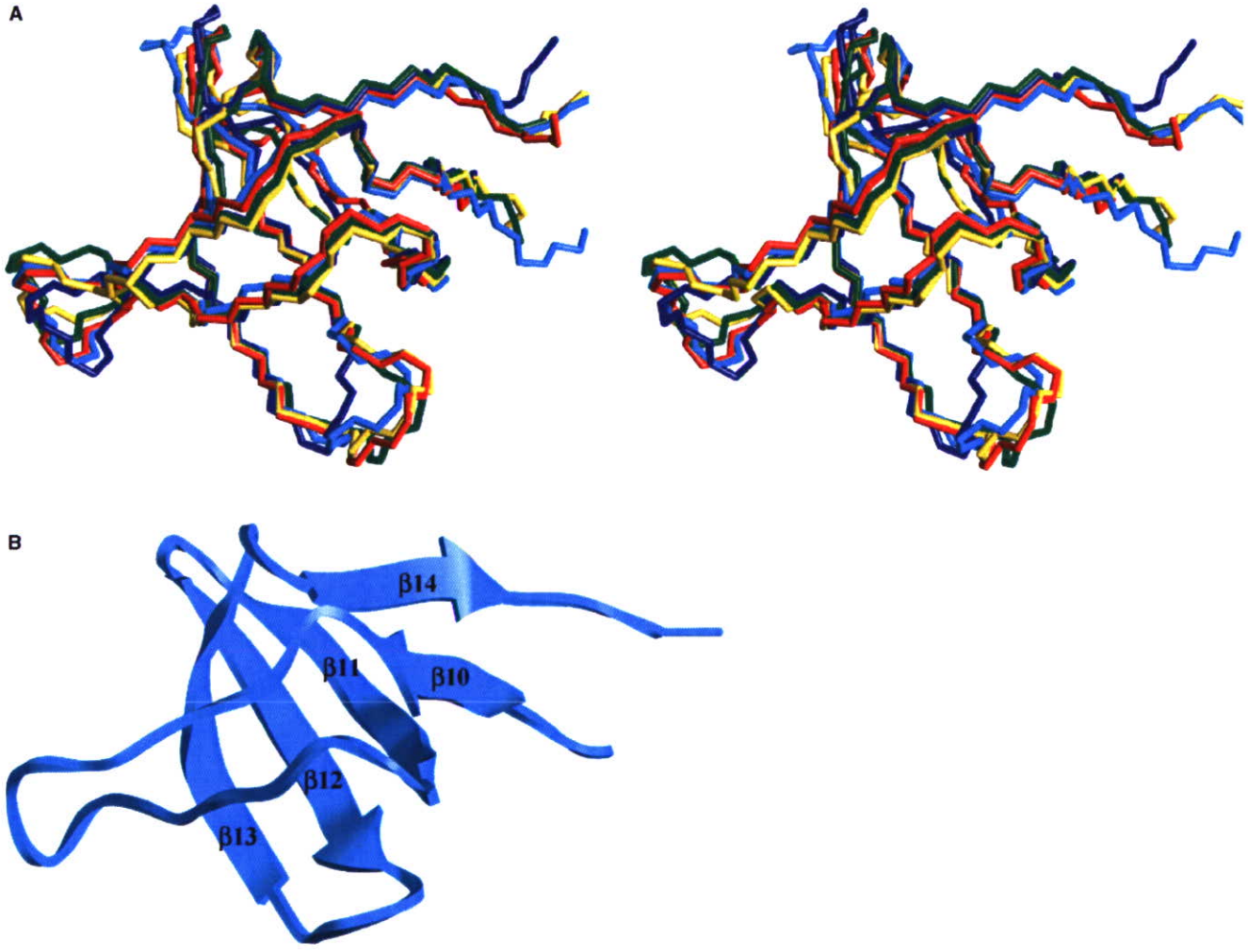

Fig. 6. Superimposition of SH3 domain of FUT8 onto various proteins containing SH3 domain. (**A**) SH3 domain of FUT8 at C-terminal was superimposed onto various proteins in a stereo view. Residues 502–562 comprise the SH3 domain of FUT8. The main chain of the SH3 domain of FUT8 is colored in cyan in this figure. Other SH3 domains were indicated in red, Abp1, the yeast actin binding protein (PDB No. 1JO8); blue, SH3 domain of neutrophil cytosol factor 4, the $p40^{phox}$, component of NADPH oxidase, (PDB No. 1W6X); green, the SH3 domain of c-Crk, a viral oncogene product (PDB No. 1CKA); and yellow, p56lck(Lck), a T-lymphocyte-specific member of the Src family of nonreceptor tyrosine kinases (PDB No. 1LCK). (**B**) A ribbon model of the SH3 domain of FUT8 is indicated.

having similarities with the FUT8 structure, and it was found that these proteins contain a SH3 domain. In particular, four proteins, yeast actin binding protein (Fazi et al. 2002), neutrophil cytosol factor 4 (Massenet et al. 2005), c-Crk, oncogene protein (Wu et al. 1995), p56 Lck, and the Src family kinase (Eck et al. 1994) were all found to have considerable similarities to the SH3 domain (residues 502–562) of FUT8, as summarized in Table I. As shown in Figure 6A, the SH3 domain of FUT8 contains a fold that is quite homologous to these proteins, regardless of the low homologies of the amino acid sequences. Because these proteins are known to interact and form a complex with a specific proline-rich peptide via the SH3 domain (Fazi et al. 2002; Massenet et al. 2005), the SH3 domain of FUT8 may be able to interact with a proline-rich peptide. SH3 domain-containing proteins are typically localized in the cytosol and mediate numerous signal-transducing pathways via critical protein–protein interactions. On the other hand, FUT8 is a type II membrane protein that is localized in the Golgi apparatus, and its catalytic domain and C-terminal SH3 domain are located in the lumen. It is not clear whether the luminal SH3 domain of FUT8 is functional in glycosyl-transfer, for example, through the selection of acceptor proteins, like the lectin domain of polypeptide α-*N*-acetylgalactosaminyltransferases (Fritz et al. 2004, 2006; Kubota et al. 2006), and the regulation of its enzymatic activity, or whether it has any other functions including localization, subunit formation or unknown functions. To elucidate the function of the SH3 domain on FUT8, further functional studies are needed and are currently in progress.

Conclusion

The overall structure of FUT8, human α1,6-fucosyltransferase, was solved and the findings indicate that the enzyme appears to have a catalytic region similar to GT-B glycosyltransferases rather than GT-A. In addition, it was found that FUT8 contains an SH3 domain at the C-terminus, which is quite similar to the SH3 domains found in other proteins but is unique in glycosyltransferase proteins. Although it would be expected that the SH3 domain of FUT8 may function to associate with substrate glycoproteins or unknown regulatory proteins, the definite significance of this domain remains to be elucidated. Consistent with earlier studies involving homology analyses and mutagenesis, the present structural and enzymatic studies of FUT8 also suggest that conserved residues in the three conserved motifs participate in the Rossmann fold and are involved in donor binding or in catalysis, thus playing a key role in the fucose-transferring reaction.

Materials and methods

Preparation of recombinant protein

FUT8 was expressed in soluble form, with a C-terminal polyhistidine tag, and purified by Ni^{2+} chelating affinity chromatography as described previously (Ihara et al. 2006). The protein was expressed using a baculovirus/insect cell expression system, as described previously (Ihara et al. 2006). Solutions of the purified proteins, at a concentration of 10 mg/mL, in 50 mM Tris–HCl buffer at pH 8.3, were used for crystallization. Protein concentrations were determined using a BCA Kit (Pierce, IL), with bovine serum albumin (BSA) as a standard.

Crystallization

Crystallization of the recombinant FUT8 was performed at 27 °C using the hanging drop vapor diffusion method. The drop contained protein at a concentration of 2.5–6.0 mg/mL in 50 mM HEPES-Na, 0.75 M lithium sulfate monohydrate, pH 7.5, and the reservoir solution contained 100 mM HEPES-Na, 1.5 M lithium sulfate monohydrate, pH 7.5. To prepare heavy atom derivatives of protein crystals, the crystals were soaked for 5 h in the presence of 10 mM potassium tetrachloroplatinate(II) in the same buffer that was used in the reservoir solution. The crystals were then transferred to a cryoprotectant solution containing 20% glycerol in the reservoir solution to prevent the formation of ice under the cryogenic environment.

X-ray data collection and structure determination

Crystals were flash-frozen in cryogenic nitrogen gas at 100 K, and data sets were then collected at the same temperature. Diffraction data for native and Pt derivative were collected using an imaging plate detector at the beamline BL44XU at SPring-8. The obtained data were indexed, integrated, and scaled using DENZO/SCALEPACK (Otwinowski et al. 1997). There were two non-isomorphous crystals, native1 and native2. The calculated R_{iso} between them was 38.5% (100–2.8 Å). The FUT8 crystal used in this study belongs to the $P6_522$ space group with one molecule per asymmetric unit. The unit cell dimensions for the native1 FUT8 crystal using structure determination are: $a = 90.46$ Å, $b = 90.46$ Å, and $c = 381.9$Å. Data collection and processing statistics for the data sets are summarized in Table II. Phases were determined by a single isomorphous replacement with anomalous scattering (SIRAS) using the data sets for native1 and Pt derivative. One clear platinum position was found on Harker sections from both the calculated difference and the anomalous Patterson map. The determined platinum position was refined using the program SHARP (de La Fortelle and Bricogne 1997). Density modification with solvent flattening was performed with the program SOLOMON (Abrahams and Leslie 1996) implemented in SHARP. The resultant experimental map using native1 data was traced and the model building was performed with the program O (Jones et al. 1991). The final model was built using native2 data and refined with program REFMAC5 (Murshudov et al. 1997) and ARP/wARP (Lamzin et al. 2001) in CCP4 suite (Collaborative Computational Project Number 4, 1994). The Ramachandran plot was also defined by PROCHECK (Lakowsky et al. 1993). Figures were produced using the UCSF Chimera program (Pettersen et al. 2004).

Cell culture

COS-1 cells were maintained in Dulbecco's modified Eagle's medium containing 10% fetal calf serum, 100 units/mL penicillin, 100 μg/mL streptomycin, and 5 g/L glucose under a humidified atmosphere of 95% air and 5% CO_2.

Construction of expression plasmids

For transient expression in COS-1 cells, a cDNA encoding human FUT8 (Yanagidani et al. 1997) was subcloned into

the *Eco*RI sites of an expression vector, pCXNII (Niwa et al. 1991). In this vector, FUT8 was expressed under the control of the β-actin promoter and the CMV enhancer.

Site-directed mutagenesis

Site-directed mutagenesis experiments were carried out using the QuikChange site directed mutagenesis kit (Stratagene, La Jolla, CA), as described previously (Ihara et al. 2004). The primers used in this study were 5′- GTCAGACGCACAGCG AAAGTGGGAACAG-3′ and 5′-CTGTTCCCACTTTCGCTG TGCGTCTGAC-3′ for replacement of Asp-368 (designated as D368A), 5′-GACGCACAGACGCAGTGGGAACAGAAG C-3′ and 5′- GCTTCTGTTCCCACTGCGTCTGTGCGTC-3′ for replacement of Lys-369 (K369A), and 5′- AAAGTGGG AACAGCAGCTGCCTTCCAT-3′ and 5′-ATGGAAGGCAG CTGCTGTTCCACTTT-3′ for replacement of Glu-373 (E373A), 5′-CCCATTGAAGAGGCAATGGTGCATGTT-3′ and 5′-AACATGCACCATTGCCTCTTCAATGGG-3′ for replacement of Tyr-382 (Y382A), 5′-GTATTTGGCCACAG CGGACCCTTCTTTATTAAAGG-3′ and 5′-CCTTTAAT AAAGAAGGGTCCGCTGTGGCCAAATAC-3′ for replacement of Asp-409 (D409A), 5′-GTATTGGCCACAGATGC GCCTTCTTTATTAAAGG-3′ and 5′-CCTTTAATAAAGAA GGCGCATCTGTGGCCAAATAC-3′ for replacement of A sp-410 (D410A), 5′-GGAGTGATCCTGGCGATACATTTTC TCTC-3′ and 5′-

GAGAGAAAATGTATCGCCAGGATCACTCC-3′ for replacement of Asp-453 (D453A), and 5′-TGTACTTTTT CAGCACAGGTCTGTCGA-3′ and 5′-TCGACAGACCTGT GCTGAAAAAGTACA-3′ for replacement of Ser-469 (S469A). The resulting mutations were verified by using BigDye® Terminator v3.1 Cycle Sequencing Kit and a DNA sequencer, ABI PRISM® 3100 Genetic Analyzer (Applied Biosystems, CA).

DNA transfection

Expression plasmids were transfected into cells by electroporation (Chu et al. 1987) using a Gene Pulser (Bio-Rad, CA), as described previously (Ihara et al. 2002). In a typical experiment, the cells were washed with HEPES-buffered saline and resuspended in the same solution. Plasmids (30 μg) were added to the cell suspension, followed by electrification. For the transient expression in Huh-6 cells, transfected cells were harvested after an appropriate growth period. The expression of FUT8 was verified by immunoblot analysis and enzyme activity assay for FUT8.

Electrophoresis and immunoblot analysis

SDS–PAGE was carried out on 8% gels, according to Laemmli (1970). Immunoblot analyses were performed as described previously (Ihara et al. 2002). The separated proteins were transferred onto a nitrocellulose membrane (PROTORAN, Schleicher & Schuell Inc., NH), and the resulting blot was blocked with 5% skim milk and 0.5% BSA in phosphate-buffered saline (PBS) containing 0.05% Tween-20. The resulting membrane was incubated with the 15C6 antibody against FUT8. The 15C6 antibody is a monoclonal antibody against human and porcine FUT8, and was obtained from Fujirebio Inc. (Tokyo, Japan). After washing with PBS containing 0.05% Tween-20, the membrane was reacted with a horseradish peroxidase -conjugated rabbit anti-(mouse IgG) Ig from Promega (Madison, WI). The immuno-reactive protein bands were visualized by HRP reaction using 4-chloro-1-naphtol and 3,3′-diaminobenzidine tetrahydrochloride (Pirece, IL) as substrates.

FUT8 activity assay

α1,6-Fucosyltransferase activity was assayed using a fluorescence-labeled sugar chain substrate, as described previously (Uozumi, Teshima et al. 1996; Ihara et al. 2006). Cell lysates were incubated at 37 °C with 10 μM of the acceptor substrate and 0.5 mM GDP-fucose as a donor in 0.1 M MES-NaOH, 1% Triton X-100 (pH 7.0). The reactions were terminated by boiling after an appropriate reaction time, and the reaction mixtures were centrifuged at 15 000*g* in a microcentrifuge for 10 min. The resulting supernatants were injected to a reversed phase HPLC equipped with TSKgel, ODS 80TM (4.6 × 150 mm) (Tosoh, Tokyo, Japan). The product and substrate were separated isocratically with 20 mM ammonium acetate buffer (pH 4.0) containing 0.15% *n*-butanol. The fluorescence of the column elute was detected with fluorescence detector (2475 Multi λ Fluorescence Detector, waters, MA) at excitation and emission wavelengths of 315 and 380 nm, respectively.

Acknowledgments

We thank Dr Pradman K. Qasba for his critical reading of the manuscript. This research was supported by The National Project on Protein Structural and Functional Analyses (Priority Research Program, Protein 3000 Project) from the Ministry of Education, Culture, Sports, Science and Technology of Japan and by The 21st Century Center of Excellence Program.

Conflict of interest statement

None declared.

Abbreviations

FUT8, mammalian α1,6-fucosyltransferase; GDP, guanosine 5′-diphosphate; GlcNAc, N-Acetylglucosamine; Ig, immunoglobulin; *N*-glycan, asparagines-linked oligosaccharide; PBS, phosphate-buffered saline

References

Abrahams JP, Leslie AGW. 1996. Methods used in the structure determination of bovine mitochondrial F1 ATPase. Acta Crystallogr D. 52: 30–42.

Becker DJ, Lowe JB. 2003. Fucose: biosynthesis and biological function in mammals. Glycobiology. 13:41R–53R.

Breton C, Oriol R, Imberty A. 1998. Conserved structural features in eukaryotic and prokaryotic fucosyltransferases. Glycobiology. 8:87–94.

Chazalet V, Uehara K, Geremia RA, Breton C. 2001. Identification of essential amino acids in the *Azorhizobium caulinodans* fucosyltransferase NodZ. J Bacteriol. 183:7067–7075.

Chiu CP, Watts AG, Lairson LL, Gilbert M, Lim D, Wakarchuk WW, Withers SG, Strynadka NC. 2004. Structural analysis of the sialyltransferase CstII from *Campylobacter jejuni* in complex with a substrate analog. Nat Struct Mol Biol. 11:163–170.

Chu G., Hayakawa H, Berg P. 1987. Electroporation for the efficient transfection of mammalian cells with DNA. Nucleic Acids Res. 15:1311–1326.

Collaborative Computational Project, Number 4. 1994. The CCP4 suite: programs for protein crystallography. Acta Crystallogr D. 50:760–763.

Couinho PM, Deleury E, Davies GJ, Henrissat B. 2003. An evolving hierarchical family classification for glycosyltransferases. J Mol Biol. 328: 307–317.

de La Fortelle E, Bricogne G. 1997. Maximum-likelihood heavy-atom parameter refinement for multiple isomorphous replacement and multiwavelength anomalous diffraction methods. Methods Enzymol. 276:472–494.

Eck MJ, Atwell SK, Shoelson SE, Harrison SC. 1994. Structure of the regulatory domains of the Src-family tyrosine kinase Lck. Nature. 368: 764–769.

Fazi B, Cope MJ, Douangamath A, Ferracuti S, Schirwitz K, Zucconi A, Drubin DG, Wilmanns M, Cesareni G, Castagnoli L. 2002. Unusual binding properties of the SH3 domain of the yeast actin-binding protein Abp1: structural and functional analysis. J Biol Chem. 277:5290–5298.

Flint J, Taylor E, Yang M, Bolam DN, Tailford LE, Martinez-Fleites C, Dodson EJ, Davis BG, Gilbert HJ, Davies GJ. 2005. Structural dissection and high-throughput screening of mannosylglycerate synthase. Nat Struct Mol Biol. 12:608–614.

Fritz TA, Hurley JH, Trinh LB, Shiloach J, Tabak LA. 2004. The beginnings of mucin biosynthesis: the crystal structure of UDP-GalNAc:polypeptide α-*N*-acetylgalactosaminyltransferase-T1. Proc Natl Acad Sci USA. 101: 15307–15312.

Fritz TA, Raman J, Tabak LA. 2006. Dynamic association between the catalytic and lectin domains of human UDP-GalNAc:polypeptide α-*N*-acetylgalactosaminyltransferase-2. J Biol Chem. 281:8613–8619.

Gastinel LN, Bignon C, Misra AK, Hindsgaul O, Shaper JH, Joziasse DH. 2001. Bovine α1,3-galactosyltransferase catalytic domain structure and its relationship with ABO histo-blood group and glycosphingolipid glycosyltransferases. EMBO J. 20:638–649.

Gastinel LN, Cambillau C, Bourne Y. 1999. Crystal structures of the bovine β4galactosyltransferase catalytic domain and its complex with uridine diphosphogalactose. EMBO J 18:3546–3557.

Gibson RP, Turkenburg JP, Charnock SJ, Lloyd R, Davies GJ. 2002. Insights into trehalose synthesis provided by the structure of the retaining glycosyltransferase OtsA. Chem Biol. 9:1337–1346.

Holm L, Sander C. 1993. Protein structure comparison by alignment of distance matrices. J Mol Biol. 233:123–138.

Ihara H, Ikeda Y, Koyota S, Endo T, Honke K, Taniguchi N. 2002. A catalytically inactive β1,4-*N*-acetylglucosaminyltransferase III (GnT-III) behaves as a dominant negative GnT-III inhibitor. Eur J Biochem. 269: 193–201.

Ihara H, Ikeda Y, Taniguchi N. 2006. Reaction mechanism and substrate specificity for nucleotide sugar of mammalian α1,6-fucosyltransferase—a large-scale preparation and characterization of recombinant human FUT8. Glycobiology. 16:333–342.

Ihara S, Miyoshi E, Nakahara S, Sakiyama H, Ihara H, Akinaga A, Honke K, Dickson RB, Lin CY, Taniguchi N. 2004. Addition of β1–6 GlcNAc branching to the oligosaccharide attached to Asn 772 in the serine protease domain of matriptase plays a pivotal role in its stability and resistance against trypsin. Glycobiology. 14:139–146.

Javaud C, Dupuy F, Maftah A, Julien R, Petit JM. 2003. The fucosyltransferase gene family: an amazing summary of the underlying mechanisms of gene evolution. Genetica. 118:157–170.

Javaud C, Dupuy F, Maftah A, Michalski JM, Oriol R, Petit JM, Julien R. 2000. Ancestral exonic organization of FUT8, the gene encoding the α6-fucosyltransferase, reveals successive peptide domains which suggest a particular three-dimensional core structure for the α6-fucosyltransferase family. Mol Biol Evol. 17:1661–1672.

Jones TA, Zou J-Y, Cowan SW, Kjeldgaard M. 1991. Improved methods for building protein models in electron density maps and the location of errors in these models. Acta Crystallogr A. 47:110–119.

Kakuda S, Shiba T, Ishiguro M, Tagawa H, Oka S, Kajihara Y, Kawasaki T, Wakatsuki S, Kato R. 2004. Structural basis for acceptor substrate recognition of a human glucuronyltransferase, GlcAT-P, an enzyme critical in the biosynthesis of the carbohydrate epitope HNK-1. J Biol Chem. 279: 22693–22703.

Kaminska J, Glick MC, Koscielak J. 1998. Purification and characterization of GDP-L-Fuc: *N*-acetyl β -D-glucosaminide α1,6fucosyltransferase from human blood platelets. Glycoconj J. 15:783–738.

Kaminska J, Wisniewska A, Koscielak J. 2003. Chemical modifications of α1,6-fucosyltransferase define amino acid residues of catalytic importance. Biochimie. 85:303–310.

Kubota T, Shiba T, Sugioka S, Furukawa S, Sawaki H, Kato R, Wakatsuki S, Narimatsu H. 2006. Structural basis of carbohydrate transfer activity by human UDP-GalNAc: polypeptide α-*N*-acetylgalactosaminyltransferase (pp-GalNAc-T10). J Mol Biol. 359:708–727.

Laemmli UK. 1970. Cleavage of structural proteins during the assembly of the head of bacteriophage T4. Nature. 227:680–685.

Lakowski RA, MacArthur MW, Moss DS, Thornton JM. 1993. PROCHECK: a program to check the stereochemical quality of protein structures. J Appl Crystallogr. 26:283–291.

Lamzin VS, Perrakis A, Wilson KS. 2001. The ARP/wARP suite for automated construction and refinement of protein models. In: Rossmann MG, Arnold Eeditors. International tables for crystallography. Volume F: Crystallography of biological macromolecules. Dordrecht: Kluwer Academic Publishers; 720–722.

Lee SH, Takahashi M, Honke K, Miyoshi E, Osumi D, Sakiyama H, Ekuni A, Wang X, Inoue S, Gu JP. *et al.*, 2006. Loss of core fucosylation of low-density lipoprotein receptor-related protein-1 impairs its function, leading to the upregulation of serum levels of insulin-like growth factor-binding protein 3 in Fut8-/- mice. J Biochem (Tokyo). 139:391–398.

Li W, Nakagawa T, Koyama N, Wang X, Jin J, Mizuno-Horikawa Y, Gu J, Miyoshi E, Kato I, Honke K, *et al.* 2006. Down-regulation of trypsinogen expression is associated with growth retardation in α1,6-fucosyltransferase-deficient mice: attenuation of proteinase-activated receptor 2 activity. Glycobiology. 16:1007–1019.

Lobsanov YD, Romero PA, Sleno B, Yu B, Yip P, Herscovics A, Howell PL. 2004. Structure of Kre2p/Mnt1p: a yeast α1,2-mannosyltransferase involved in mannoprotein biosynthesis. J Biol Chem. 279:17921–17931.

Longmore GD, Schachter H. 1982. Product-identification and substrate-specificity studies of the GDP-L-fucose: 2-acetamido-2-deoxy-β-D-glucoside (FUC goes to Asn-linked GlcNAc) 6-α-L-fucosyltransferase in a Golgi-rich fraction from porcine liver. Carbohydr Res. 100:365–392.

Martinez-Duncker I, Mollicone R, Candelier JJ, Breton C, Oriol R. 2003. A new superfamily of protein-*O*-fucosyltransferases, α2-fucosyltransferases, and α6-fucosyltransferases: phylogeny and identification of conserved peptide motifs. Glycobiology. 13:1C–5C.

Massenet C, Chenavas S, Cohen-Addad C, Dagher MC, Brandolin G, Pebay-Peyroula E, Fieschi F. 2005. Effects of p47phox C terminus phosphorylations on binding interactions with p40phox and p67phox. Structural and functional comparison of p40phox and p67phox SH3 domains. J Biol Chem. 280:13752–13761.

Miyoshi E, Noda K, Ko JH, Ekuni A, Kitada T, Uozumi N, Ikeda Y, Matsuura N, Sasaki Y, Hayashi N, *et al.* 1999. Overexpression of α1–6 fucosyltransferase in hepatoma cells suppresses intrahepatic metastasis after splenic injection in athymic mice. Cancer Res. 59:2237–2243.

Miyoshi E, Noda K, Yamaguchi Y, Inoue S, Ikeda Y, Wang W, Ko JH, Uozumi N, Li W, Taniguchi N. 1999. The α1–6-fucosyltransferase gene and its biological significance. Biochim Biophys Acta. 1473:9–20.

Miyoshi E, Taniguchi N. 2002. α6-fucosyltransferase (FUT8). In: Taniguchi N, Honke K, Fukuda M editors. Handbook of glycosyltransferase and related genes. Tokyo: Springe. 259–263.

Miyoshi E, Uozumi N, Noda K, Hayashi N, Hori M, Taniguchi N. 1997. Expression of α1–6 fucosyltransferase in rat tissues and human cancer cell lines. Int J Cancer. 72:1117–1121.

Mulichak AM, Losey HC, Walsh CT, Garavito RM. 2001. Structure of the UDP-glucosyltransferase GtfB that modifies the heptapeptide aglycone in the biosynthesis of vancomycin group antibiotics. Structure. 9:547–557.

Murshudov GN, Vagin AA, Dodson EJ. 1997. Refinement of macromolecular structures by the maximum-likelihood method. Acta Crystallogr D Biol Crystallogr. 53:240–255.

Nakakita S, Menon KK, Natsuka S, Ikenaka K, Hase S. 1999. β1-4Galactosyltransferase activity of mouse brain as revealed by analysis of brain-specific complex-type *N*-linked sugar chains. J Biochem (Tokyo). 126:1161–1169.

Ni L, Sun M, Yu H, Chokhawala H, Chen X, Fisher AJ. 2006. Cytidine 5'-monophosphate (CMP)-induced structural changes in a multifunctional sialyltransferase from *Pasteurella multocida*. Biochemistry. 45: 2139–2148.

Niwa H, Yamamura K, Miyazaki J. 1991. Efficient selection for high-expression transfectants with a novel eukaryotic vector. Gene. 108: 193–199.

Noda K, Miyoshi E, Uozumi N, Yanagidani S, Ikeda Y, Gao C, Suzuki K, Yoshihara H, Yoshikawa K, Kawano K, *et al.* 1998. Gene expression of α1–6 fucosyltransferase in human hepatoma tissues: a possible implication for increased fucosylation of α-fetoprotein. Hepatology. 28: 944–952; Erratum in, 1999. Hepatology. 29:301.

Okajima T, Xu A, Lei L, Irvine KD. 2005. Chaperone activity of protein *O*-fucosyltransferase 1 promotes notch receptor folding. Science. 307: 1599–1603.

Okazaki A, Shoji-Hosaka E, Nakamura K, Wakitani M, Uchida K, Kakita S, Tsumoto K, Kumagai I, Shitara K. 2004. Fucose depletion from human IgG1 oligosaccharide enhances binding enthalpy and association rate between IgG1 and FcγRIIIa. J Mol Biol. 336:1239–1249.

Oriol R, Mollicone R, Cailleau A, Balanzino L, Breton C. 1999. Divergent evolution of fucosyltransferase genes from vertebrates, invertebrates, and bacteria. Glycobiology. 9:324–334.

Oriol R, Mollicone R. 2002. α2-fucosyltransferase (FUT1, FUT2, and Sec1). In: Taniguchi N, Honke K, Fukuda M editors. Handbook of glycosyltransferase and related genes. Tokyo: Springer. 205–217.

Otwinowski Z, Minor W. 1997. Processing of X-ray diffraction data collected in oscillation mode. Methods Enzymol. 276:307–326.

Pak JE, Arnoux P, Zhou S, Sivarajah P, Satkunarajah M, Xing X, Rini JM. 2006. X-ray crystal structure of leukocyte type core2 β1,6-*N*-acetylglucosaminyltransferase. Evidence for a convergence of metal ion-independent glycosyltransferase mechanism. J Biol Chem. 281:26693–26701.

Paschinger K, Staudacher E, Stemmer U, Fabini G, Wilson IB. 2005. Fucosyltransferase substrate specificity and the order of fucosylation in invertebrates. Glycobiology. 15:463–474.

Patenaude SI, Seto NO, Borisova SN, Szpacenko A, Marcus SL, Palcic MM, Evans SV. 2002. The structural basis for specificity in human ABO(H) blood group biosynthesis. Nat Struct Biol. 9:685–690.

Pedersen LC, Dong J, Taniguchi F, Kitagawa H, Krahn JM, Pedersen LG, Sugahara K, Negishi M. 2003. Crystal structure of an α1,4-*N*-acetylhexosaminyltransferase (EXTL2), a member of the exostosin gene family involved in heparan sulfate biosynthesis. J Biol Chem. 278: 14420–14428.

Pedersen LC, Tsuchida K, Kitagawa H, Sugahara K, Darden TA, Negishi M. 2000. Heparan/chondroitin sulfate biosynthesis. Structure and mechanism of human glucuronyltransferase I. J Biol Chem. 275:34580–34585.

Perrakis A, Harkiolaki M, Wilson KS, Lamzin VS. 2001. ARP/wARP and molecular replacement. Acta Crystallogr D Biol Crystallogr. 57: 1445–1450.

Pettersen EF, Goddard TD, Huang CC, Couch GS, Greenblatt DM, Meng EC, Ferrin TE. 2004. UCSF Chimera—a visualization system for exploratory research and analysis. J Comput Chem. 25:1605–1612.

Qasba PK, Ramakrishnan B, Boeggenman E. 2005. Substrate-induced conformational changes in glycosyltransferases. Trends Biochem Sci. 30:53–62.

Ramakrishnan B, Boeggeman E, Ramasamy V, Qasba PK. 2004. Structure and catalytic cycle of β-1,4-galactosyltransferase. Curr Opin Struct Biol. 14:593–600.

Ramasamy V, Ramakrishnan B, Boeggeman E, Qasba PK. 2003. The role of tryptophan 314 in the conformational changes of beta1,4-galactosyltransferase-1. J Mol Biol. 331:1065–1076.

Shields RL, Lai J, Keck R, O'Connell LY, Hong K, Meng YG, Weikert SH, Presta LG. 2002. Lack of fucose on human IgG1 *N*-linked oligosaccharide improves binding to human FcγRIII and antibody-dependent cellular toxicity. J Biol Chem. 277:26733–26740.

Shinkawa T, Nakamura K, Yamane N, Shoji-Hosaka E, Kanda Y, Sakurada M, Uchida K, Anazawa H, Satoh M, Yamasaki M, *et al.* 2003. The absence of fucose but not the presence of galactose or bisecting *N*-acetylglucosamine of human IgG1 complex-type oligosaccharides shows the critical role of enhancing antibody-dependent cellular cytotoxicity. J Biol Chem. 278:3466–3473.

Staudacher E, Altmann F, Wilson IB, Marz L. 1999. Fucose in *N*-glycans: from plant to man. Biochim Biophys Acta. 473:216–236.

Staudacher E, Marz L. 1998. Strict order of (Fuc to Asn-linked GlcNAc) fucosyltransferases forming core-difucosylated structures. Glycoconj J. 15:355–360.

Stavropoulos P, Blobel G, Hoelz A. 2006. Crystal structure and mechanism of human lysine-specific demethylase-1. Nat Struct Mol Biol. 13: 626–632.

Takahashi T, Ikeda Y, Tateishi A, Yamaguchi Y, Ishikawa M, Taniguchi N. 2000. A sequence motif involved in the donor substrate binding by α1,6-fucosyltransferase: the role of the conserved arginine residues. Glycobiology. 10:503–510.

Taketa K, Endo Y, Sekiya C, Tanikawa K, Kojii T, Taga H, Satomura S, Matsuura S, Kawai T, Hirai H. 1993. A collaborative study for the evaluation of lectin-reactive α-fetoproteins in early detection of hepatocellular carcinoma. Cancer Res. 53:5419–5423.

Taniguchi N, Miyoshi E, Jianguo G, Honke K, Matsumoto A. 2006. Decoding sugar functions by identifying target glycoproteins. Curr Opin Struct Biol. 16:561–566.

Tarbouriech N, Charnock SJ, Davis GJ. 2001. Three-dimentional structures of the Mn and Mg dTDP complexes of the family GT-2glycosyltransferase SpsA: a comparison with related NDP-sugar glycosyltransferases. J Mol Biol. 314:655–661.

Thoden JB, Huang X, Raushel FM, Holden HM. 1999. The small subunit of carbamoyl phosphate synthetase: snapshots along the reaction pathway. Biochemistry. 38:16158–16166.

Ünligil UM, Rini JM. 2000. Glycosyltransferase structure and mechanism. Curr Opin Struct Biol. 10:510–517.

Ünligil UM, Zhou S, Yuwaraj S, Sarkar M, Schachter H, Rini JM. 2000. X-ray crystal structure of rabbit *N*-acetylglucosaminyltransferase I: catalytic mechanism and a new protein superfamily. EMBO J. 19:5269–5280.

Uozumi N, Teshima T, Yamamoto T, Nishikawa A, Gao YE, Miyoshi E, Gao CX, Noda K, Islam KN, Ihara Y, *et al.* 1996. A fluorescent assay method for GDP-L-Fuc: *N*-acetyl-β-D-glucosaminide α1-6fucosyltransferase activity, involving high performance liquid chromatography. J Biochem (Tokyo). 120:385–392.

Uozumi N, Yanagidani S, Miyoshi E, Ihara Y, Sakuma T, Gao CX, Teshima T, Fujii S, Shiba T, Taniguchi N. 1996. Purification and cDNA cloning of porcine brain GDP-L-Fuc:*N*-acetyl-β-D-glucosaminide α1,6fucosyltransferase. J Biol Chem. 271:27810–27817.

Voynow JA, Kaiser RS, Scanlin TF, Glick MC. 1991. Purification and characterization of GDP-L-fucose-*N*-acetyl beta-D-glucosaminide alpha 1-6fucosyltransferase from cultured human skin fibroblasts. Requirement of a specific biantennary oligosaccharide as substrate. J Biol Chem. 266: 21572–21577.

Wang X, Gu J, Ihara H, Miyoshi E, Honke K, Taniguchi N. 2006. Core fucosylation regulates epidermal growth factor receptor-mediated intracellular signaling. J Biol Chem. 281:2572–2577.

Wang X, Inoue S, Gu J, Miyoshi E, Noda K, Li W, Mizuno-Horikawa Y, Nakano M, Asahi M, Takahashi M, *et al.* 2005. Dysregulation of TGF-β1 receptor activation leads to abnormal lung development and emphysema-like phenotype in core fucose-deficient mice. Proc Natl Acad Sci U S A. 102:15791–15796.

White A, Rose DR. 1997. Mechanism of catalysis by retaining β-glycosyl hydrolases. Curr Opin Struct Biol. 7:645–651.

Wilson JR, Williams D, Schachter H. 1976. The control of glycoprotein synthesis: *N*-acetylglucosamine linkage to a mannose residue as a signal for the attachment of L-fucose to the asparagine-linked *N*-acetylglucosamine residue of glycopeptide from alpha1-acid glycoprotein. Biochem Biophys Res Commun. 72:909–916.

Wu X, Knudsen B, Feller SM, Jie Zheng J, Sali A, Cowburn D, Hanafusa H, Kuriyan J. 1995. Structural basis for the specific interaction of lysine-containing proline-rich peptides with the N-terminal SH3 domain of c-Crk. Structure. 3:215–226.

Yanagidani S, Uozumi N, Ihara Y, Miyoshi E, Yamaguchi N, Taniguchi N. 1997. Purification and cDNA cloning of GDP-L-Fuc: *N*-acetyl-β-D-glucosaminide:α1–6 fucosyltransferase (α1–6 FucT) from human gastric cancer MKN45 cells. J Biochem (Tokyo). 121:626–632.

Zarembinski TI, Hung L-W, Mueller-Dieckmann HJ, Kim K-K, Yokota H, Kim R, Kim S-H. 1998. Structure-based assignment of the biochemical function of a hypothetical protein: a test case of structural genomics. Proc Natl Acad Sci U S A. 95:15189–15193.

Zechel DL, Withers SG. 2001. Dissection of nucleophilic and acid–base catalysis in glycosidases. Curr Opin Chem Biol. 5:643–649.

Zhao Y, Itoh S, Wang X, Isaji T, Miyoshi E, Kariya Y, Miyazaki K, Kawasaki N, Taniguchi N, Gu J. 2006. Deletion of core fucosylation on α3β1 integrin down-regulates its functions. J Biol Chem. 281:38343–38350.

Glycobiology vol. 17 no. 6 pp. 655–662, 2007
doi:10.1093/glycob/cwm022
Advance Access publication on February 26, 2007

Introduction of bisecting GlcNAc in *N*-glycans of adenylyl cyclase III enhances its activity

Wei Li[2], Motoko Takahashi[3], Yukinao Shibukawa[2], Shunichi Yokoe[2], Jianguo Gu[4], Eiji Miyoshi[2], Koichi Honke[5], Yoshitaka Ikeda[3], and Naoyuki Taniguchi[1,6]

[2]Department of Biochemistry, Osaka University Graduate School of Medicine, 2-2 Yamadaoka, Suita, Osaka 565-0871, Japan; [3]Division of Molecular Cell Biology, Department of Biomolecular Sciences, Saga University Faculty of Medicine, 5-1-1 Nabeshima, Saga 849-8501, Japan; [4]Division of Regulatory Glycobiology, Institute of Molecular Biomembrane and Glycobiology, Tohoku Pharmaceutical University, Sendai, Miyagi 981-8558, Japan; [5]Department of Biochemistry, Kochi Medical School, Nangoku, Kochi 783-8505, Japan; and [6]Department of Disease Glycomics, Research Institute for Microbial Diseases, 4th Floor, Center for Advanced Science & Innovation, Osaka University, 2-1 Yamadaoka, Suita, Osaka 565-0871, Japan

Received on January 9, 2007; revised on February 16, 2007; accepted on February 19, 2007

Adenylyl cyclases (ACs) catalyze the synthesis of cAMP in response to extracellular and intracellular signals and are responsible for a wide variety of biological activities including cell growth, differentiation, and metabolism. There are nine, currently known, isoforms of transmembrane ACs, and the primary structure of the catalytic unit and the potential *N*-glycosylation sites are highly conserved among them. The enzyme β1,4-*N*-acetylglucosaminyltransferase III (GnT-III) catalyzes the addition of a bisecting *N*-acetylglucosamine (GlcNAc) to *N*-glycans. We have been studying the function of GnT-III on signaling molecules. In this study, we report on the effects of a bisecting GlcNAc on AC signaling. We established GnT-III stable expressing cell lines of Neuro-2a mouse neuroblastoma cells and B16 mouse melanoma cells. Forskolin-induced AC activation and downstream signaling, such as the synthesis of cAMP and the phosphorylation of transcriptional factor CRE-binding protein were upregulated in the GnT-III transfectants compared with mock transfectants or a dominant negative mutant of GnT-III-transfected cells. Since endogenous AC expression levels in Neuro-2a and B16 cells were too low to permit the glycosylation status to be examined, AC type III (ACIII) was overexpressed in a stable expression system using Flp-In-293 cells. The *N*-glycans of ACIII in the GnT-III transfectants were confirmed to be modified by the introduction of a bisecting GlcNAc, and AC activity was found to be significantly up-regulated in the GnT-III transfectants. Thus, the structure of *N*-glycans of ACIII regulates its enzymatic activity and downstream signaling.

[1]To whom correspondence should be addressed; Tel: +81-6-6879-4137; Fax: +81-6-6879-4137; e-mail address: tani52@wd5.so-net.ne.jp

Key words: adenylyl cyclase/bisecting GlcNAc/glycosylation/GnT-III/*N*-glycan

Introduction

Adenylyl cyclases (ACs) catalyze the synthesis of cAMP in response to extracellular and intracellular signals and are involved in wide variety of biological activities including cell growth, differentiation, and metabolism. Nine isoforms of transmembrane ACs and a soluble AC have been isolated and analyzed to date, revealing diverse regulation by G-proteins, Ca^{2+}, protein kinase A (PKA), and protein kinase C (PKC) (Sunahara et al. 1996; Smit and Iyengar 1998; Tang and Hurley 1998; Sunahara and Taussig 2002). All membrane-bound ACs contain two hydrophobic regions that comprise six transmembrane helices and three large cytoplasmic domains, and the primary structure of catalytic unit is conserved among ACs. Although the amino acid sequences in the extracellular regions vary among AC isozymes, potential *N*-glycosylation sites are highly conserved among them and are located on predicted extracellular loop 5 and/or loop 6, suggesting the importance of glycosylation in the function of ACs.

N-glycans on glycoproteins regulate their function in various manners; for example, *N*-glycans affect the intracellular transport of membrane proteins, the ligand binding rate of receptors, dimerization status or the endocytosis rate of receptors. The mechanisms of this regulation have been studied, and it was proposed that *N*-glycans alter the physico-chemical properties of core proteins, such as conformation, flexibility, and hydrophilicity, and thus regulate protein sorting, stability, and protein–protein interactions (Dennis et al. 1999; Rudd et al. 2001; Helenius and Aebi 2004; Freeze and Aebi 2005; Taniguchi et al. 2006). Lectin or lectin-like molecules, which recognize the peripheral structures of *N*-glycans, are also involved in the regulation of glycoproteins (Partridge et al. 2004; Ohtsubo et al. 2005). *N*-glycans have a common core structure, and their branching patterns are determined by glycosyltransferase enzymes. β1,4-*N*-acetylglucosaminyltransferase III (GnT-III) is a glycosyltransferase that catalyzes the addition of a bisecting GlcNAc residue to the β-mannoside of the trimannose core in *N*-glycans (Narasimhan 1982; Nishikawa et al. 1992; Taniguchi et al. 1999; Stanley 2002). GnT-III is known to suppress the elongation of *N*-glycans, since other glycosyltransferases such as GnT-IV and GnT-V, both of which are involved in the formation of multiantennary sugar chains, are not able to act on *N*-glycans that contain a bisecting GlcNAc (Schachter 1986; Gu et al. 1993).

To identify the role of *N*-glycans in the signaling pathway, we employed a promoter–reporter assay and found that the

forskolin-induced activation of the cAMP response element (CRE) was enhanced in the GnT-III transfectants. We observed that the forskolin-induced catalytic activity of AC was significantly increased in GnT-III-transfected Neuro-2a cells and B16 cells, compared with control cells. Exogenously expressed AC type III (ACIII) activity was also up-regulated by introduction of GnT-III, and it was confirmed that the *N*-glycan of AC was modified by a bisecting GlcNAc. Our findings demonstrate that ACIII activity is up-regulated by GnT-III transfection, and the mechanism by which AC activity is regulated by *N*-glycans is proposed.

Results

Increase in forskolin-induced downstream signaling in GnT-III-transfected Neuro-2a cells

Previous studies have demonstrated that glycosylation patterns regulate the function of many types of signaling molecules. We examined transcription from the elements of AP-1, CRE, heat shock element (HSE), Myc, NF-κB in several cell lines induced by various types of stimulation using a promoter–reporter assay method. Among those elements, we found that transcription from CRE was elevated by 2-fold in GnT-III-transfected Neuro-2a cells when stimulated with 10 μM forskolin at 37 °C for 4 h (data is not shown). We confirmed that the phosphorylation of CRE- binding protein (CREB) at Ser-133 was enhanced in the GnT-III transfectants compared with mock transfectants or the D323A dominant negative mutant of GnT-III-transfected cells (Figure 1A). Since forskolin stimulates ACs that synthesize cAMP, leading to the activation of PKA and the phosphorylation of CREB, we then examined AC activity and cellular cAMP levels in Neuro-2a cells. As shown in Figure 1B, forskolin-induced AC activation was significantly up-regulated in the GnT-III transfectants. It was also observed that cAMP in the GnT-III transfectants was significantly increased compared with control cells (Figure 1C).

To determine whether similar phenomenon could be observed in other cell lines, we examined B16 cells and found that forskolin-induced AC activation and CREB phosphorylation were also elevated in GnT-III-transfected B16 cells (Figure 2A and B).

Identification of AC isoforms up-regulated by GnT-III transfection in Neuro-2a cells and B16 cells

Since there are nine, currently known, membrane-bound AC isoforms and one soluble isoform, we attempted to determine which isoform(s) is (are) affected by GnT-III overexpression. RT–PCR was carried out using Neuro-2a cells and B16 cells, and, as shown in Figure 3, ACIII, -VI, -VII, and -IX are common in those cell lines. As reported previously, ACIII, -VI, and -VIII are glycoproteins, and ACIX is insensitive to forskolin (Premont et al. 1996); thus we assumed that ACIII and/or ACVI might be affected by GnT-III. We examined the function of *N*-glycan of ACIII in the following experiments.

Establishment of Flp-In 293 cells stably expressing ACIII

Since endogenous AC expression levels in Neuro-2a and B16 cells were too low to examine the glycosylation status, we established ACIII stable expression cell lines using Flp-In

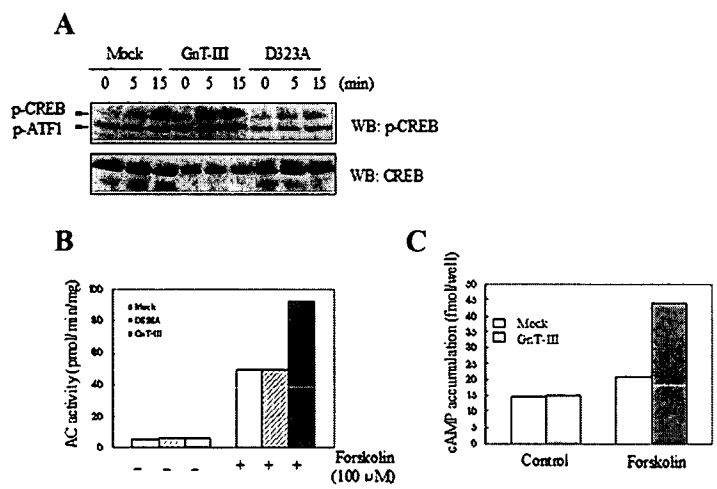

Fig. 1. Forskolin-induced AC activation and downstream signaling is enhanced in β1, 4-*N*-acetylglucosaminyltransferase III (GnT-III)-transfected Neuro-2a cells. **(A)** The time course for forskolin-induced CRE-binding protein (CREB) phosphorylation in GnT-III-overexpressed Neuro-2a cells. Cells were cultured in a 6-well dish overnight until reaching 80% confluence. After serum starvation for 7 h, the cells were stimulated by treatment with 10 μM of forskolin for 0, 5, 15 min. After washing with ice-cold phosphate-buffered saline (PBS), the cells were harvested in 100 μL lysis buffer containing proteinase inhibitors. The cell lysates were subjected to 10% SDS polyacrylamide gel electrophoresis (PAGE) and western blotting was performed using a specific anti-phospho-CREB antibody (upper panel) and anti-CREB-antibody (lower panel). Phosphorylated ATF1 (p-ATF1), a protein related to CREB, can also be detected by the anti-phospho-CREB antibody. GnT-III, wild-type GnT-III transfectants; D323A, D323A dominant negative mutant of GnT-III transfectants. **(B)** Forskolin-induced AC activation is enhanced in GnT-III-overexpressed Neuro-2a cells. For each reaction, 10 μg membrane fractions were prepared, treated with or without 100 μM forskolin at 30 °C for 20 min, and AC activity was determined as described in the *Materials and methods* section. The enzymatic product, ^{32}P-cAMP, was separated by alumina column chromatography and measured by scintillation counting. The figure shows one representative experiment of three independent experiments. **(C)** Forskolin-induced elevation of cellular cAMP is up-regulated in GnT-III-transfected Neuro-2a cells. Cells were cultured in 96-well dish overnight until 80% confluence. After cells were stimulated with forskolin (10 μM) at 37 °C for 20 min, the cellular cAMP were determined by a Biotrak cAMP enzyme immunoassay kit as described in the *Materials and methods* section. The figure shows one representative experiment of three independent experiments.